HW-67370

UC-25, Metals, Ceramics, and Materials
(TID-4500, 16th Ed.)

MECHANISMS AND KINETICS OF URANIUM CORROSION AND URANIUM CORE FUEL ELEMENT RUPTURES IN WATER AND STEAM

By

V. H. Troutner

Materials Development
Reactor and Fuels Research and Development
Hanford Laboratories Operation

July 21, 1960

HANFORD ATOMIC PRODUCTS OPERATION
RICHLAND, WASHINGTON

Work performed under Contract No. AT(45-1)-1350 between the Atomic Energy Commission and General Electric Company

Printed by/for the U. S. Atomic Energy Commission

Printed in USA. Price $2.00. Available from the
Office of Technical Services
Department of Commerce
Washington 25, D. C.

DISCLAIMER

ABSTRACT

The mechanisms and kinetics of uranium corrosion and fuel element ruptures were investigated in water and steam at 170 C to 500 C and pressures from 100 to 2800 psig. The fuel element samples were coextruded Zircaloy-clad uranium-core rods and tubes which were defected prior to exposure. Uranium corrosion was found to be the sum of two processes; direct oxidation by water, and oxidation of uranium hydride intermediate. Fuel element ruptures occur in two stages; an initial induction period followed by an accelerating corrosion of the core causing the cladding to blister, swell, and fracture. Uranium corrosion and fuel element ruptures were examined with respect to the following parameters: temperature, pressure, steam versus liquid water, heat treatment, carbon content of uranium, zirconium content of uranium, cladding thickness, fuel geometry, annular spacings, defect geometry and size, coolant flow, hydriding of Zircaloy components, and irradiation effects.

TABLE OF CONTENTS

LIST OF FIGURES

LIST OF FIGURES (contd.)

LIST OF FIGURES (contd.)

LIST OF FIGURES (contd.)

MECHANISM AND KINETICS OF URANIUM CORROSION AND URANIUM CORE FUEL ELEMENT RUPTURES IN WATER AND STEAM

INTRODUCTION

Uranium is a very reactive metal in water and steam at elevated temperatures. When nuclear reactor designs call for metallic uranium fuel element cores and water cooling, the question naturally arises as to what will happen in the event of a fuel cladding failure which permits hot water to come in contact with the hot uranium metal. Since it is certain that fuel element failures will occur in spite of careful preparations and handling, it is necessary to know the kinetics and mechanism of failure in order to determine the hazard to the reactor and personnel, the proper rupture detection system, and the best reactor operating procedures to follow.

Uranium reacts with water to form uranium dioxide and hydrogen, $U + 2H_2O \longrightarrow UO_2 + 2H_2$. The reaction proceeds at a linear rate which increases with increasing temperature. The temperature dependence of this reaction, as determined by several investigators,[1-5] is shown in Figure 1. It can be seen that the reaction rate is quite sensitive to temperature, ranging from 0.001 mil/minute at 100 C to 2 mils/minute at 300 C.

Under certain conditions the hydrogen formed by the uranium-water reaction will react with the uranium to form the trihydride, $U + 3/2\ H_2 \longrightarrow UH_3$. The rate of this reaction has been represented (for dry gas) by the equation,[6]

$$(\text{rate}) = K(P - P_D)^{2.5}$$

where K = rate constant

P = hydrogen pressure

P_D = dissociation pressure of UH_3

The rate constant, K, increases with increasing temperature, but the difference, $P - P_D$, decreases with increasing temperature for a given value of P. The net result of these two effects is that the rate of hydride formation is maximum near 225 C and decreases with increasing or decreasing temperature as shown in Figure 2.[7]

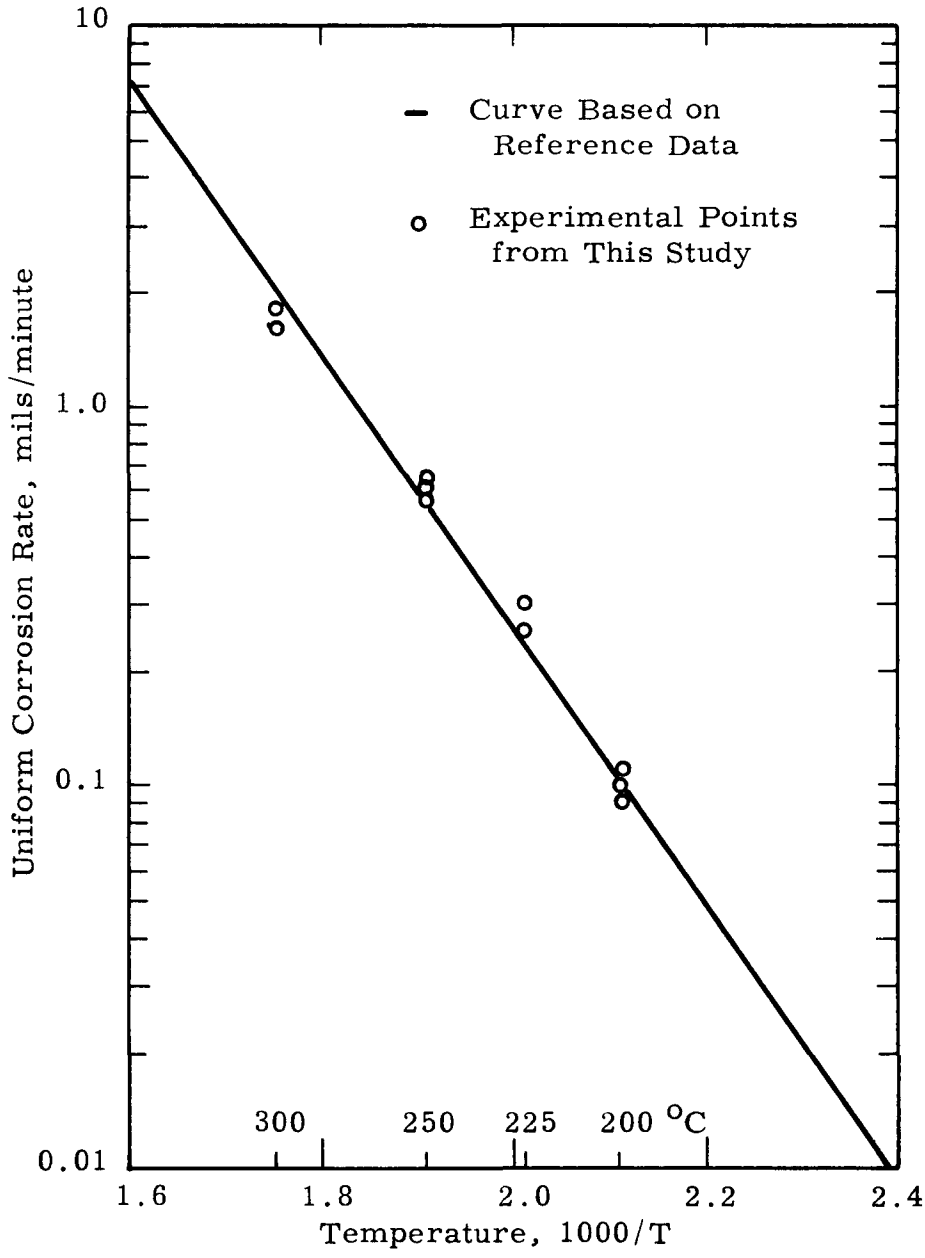

FIGURE 1

Uniform Aqueous Corrosion Rates of Uranium

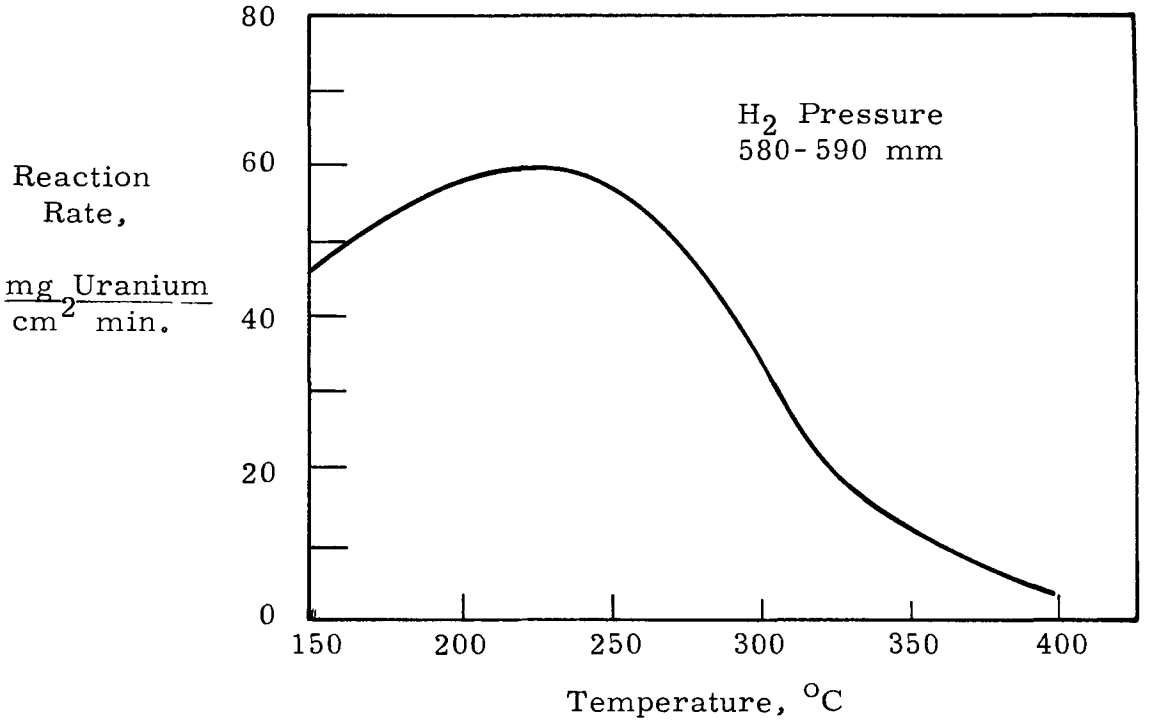

FIGURE 2

Temperature Dependence of Uranium Hydride Reaction

In order to evaluate the behavior of a fuel element rupture and the hazards involved, it is necessary to understand the mechanism of uranium corrosion and the effects of the important parameters. Economics and availability of test facilities dictate that most of the experimental work be done on unirradiated samples in autoclaves. The picture is completed by combining these data with less abundant data obtained in flow loops and irradiated rupture test facilities.

The corrosion of bare uranium represents a fairly simple system, the understanding of which is basic to the problem of fuel element ruptures. The rupture of an assembled fuel element in a process tube represents a much more complex system which introduces many additional parameters of behavior.

OBJECTIVES

It was the purpose of this study to investigate the corrosion of bare uranium and the ruptures of assembled coextruded, Zircaloy-clad fuel elements in water and steam at elevated temperatures. The work was performed in autoclaves on unirradiated samples. A further purpose was to compare the results with those obtained in flow loops and on irradiated samples. This report summarizes and augments a series of eight interim reports.[8-15]

EXPERIMENTAL

The work was performed in hydrogen-monitored quick-heat, quick-cool autoclaves. Tests with the smaller samples in water were conducted in a 1.5 inch ID, 300 ml capacity autoclave which was induction-heated and water-quenched. Test facilities for the larger samples, for steam exposures, and for direct viewing, are described in HW-64111.[16] The hydrogen collection and measuring system is also described in this report.

Test samples were of two types; open-end samples, and defected fuel element samples. The open-end samples consisted of one-inch lengths of coextruded Zircaloy-2 clad rods with the ends ground flat exposing the uranium core. Uniform corrosion penetration of these samples was measured

directly with a micrometer, the cladding serving as a reference point of the original surface. The defected fuel element samples consisted of two- to three-inch lengths of coextruded rod and tubing with unbonded welded end-closures. These samples were defected prior to testing with a pinhole drilled in through the cladding to the core, at the center of the fuel element. The sample and defect dimensions are mentioned in the discussion of the tests. The various kinds of samples are diagrammed in cross section in Figure 3.

During each test exposure, the hydrogen liberated by the corroding uranium was continuously collected and the amount recorded. After each test the sample was rinsed in water, cleaned in 50 per cent HNO_3 - 0.5 per cent HF to remove the uranium oxide, and weighed. The hydrogen collection curves were converted to uranium corrosion curves using the conversion factor obtained by dividing the total weight loss by the total hydrogen collected.

URANIUM CORROSION MECHANISM AND KINETICS

Type of Results

The corrosion of uranium was studied using the open-end samples. Three types of results were obtained, as depicted in Figure 4.

Some samples corroded in water in a very uniform manner, as in Figure 4A, with little or no pitting of the corroded surface. In this case, the penetration was measured directly as the distance from the edge of the cladding to the corroded uranium surface.

In many of the tests in lower temperature water, the attack was nonuniform as in Figure 4B. Although this type of attack resulted in deep pitting and distortion of the sample, there were at least small areas of plateaus or corroded surface parallel to the original surface. It was found that penetration rates based on measurement of the distance from these plateaus to the edge of the cladding agreed with the uniform oxidation rates available from the literature (given in Figure 1). This led to the conclusion that even where the attack was predominantly nonuniform, there was always a component of uniform corrosion present.

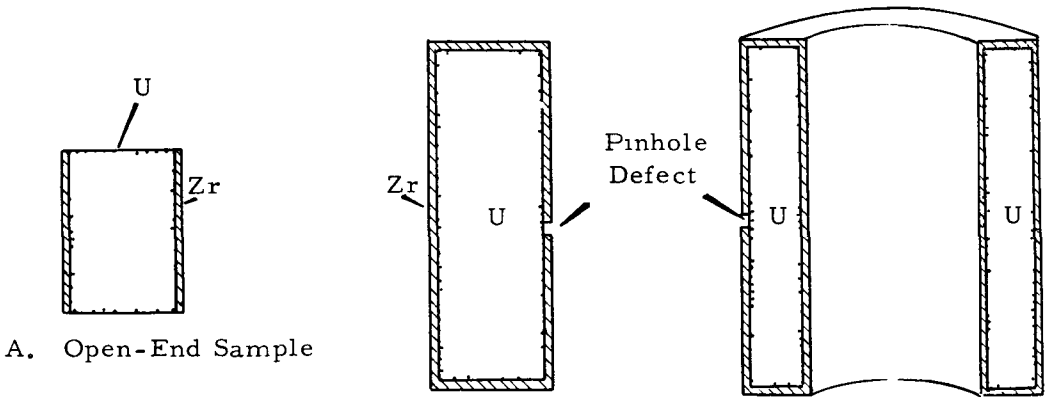

A. Open-End Sample

B. Defected Rod Element

C. Defected Tube Element

FIGURE 3

Test Samples

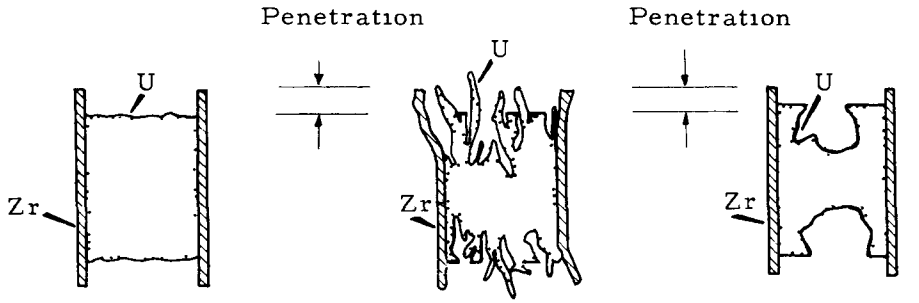

4A. Uniform Corrosion in Water

4B. Non-Uniform Corrosion in Water

4C. Corrosion in Steam

FIGURE 4

Type of Results

In steam, the attack appeared as in Figure 4C, deeply corroded cavities with some flat areas or plateaus indicative of uniform corrosion.

For all samples there were two corrosion rates obtained; the uniform penentration rate based on measurement of the distance from the plateaus to the edge of the cladding, and the over-all corrosion rate based on the hydrogen collection data and total weight loss.

Corrosion of Ingot Uranium in Water

Most of the corrosion studies were conducted with ingot uranium containing about 300 ppm carbon. The samples are shown after exposure in Figure 5. The two forms of attack, uniform and nonuniform, can be clearly seen. The extent of nonuniform attack increased with increasing pressure and decreasing temperature (over the range studied). The contribution of uniform penetration increased with increasing temperature and was insensitive to pressure. The uniform penetration rates are in good agreement with uniform oxidation rates available in the literature. Uniform corrosion penetration data are given in Table I.

TABLE I

UNIFORM CORROSION PENETRATION

Temperature ° C	Pressure psig	Exposure Minutes	Penetration mils	Penetration Rate mils/min	Literature Rate(1-5) mils/min
300	2250	61	111.0	1.82*	2.0*
300	1500	52	82.5	1.59*	
250	2250	91	58.6	0.64	0.56
250	1500	98	59.8	0.61	
250	750	99	56.6	0.57	
225	2250	134	40.8	0.30	0.25
225	750	170	44.6	0.26	
200	2250	319	29.1	0.091	0.10
200	1500	316	34.1	0.110	
200	750	329	32.4	0.099	

* The somewhat low values obtained at 300 C compared to the literature rate are discussed in a later section.

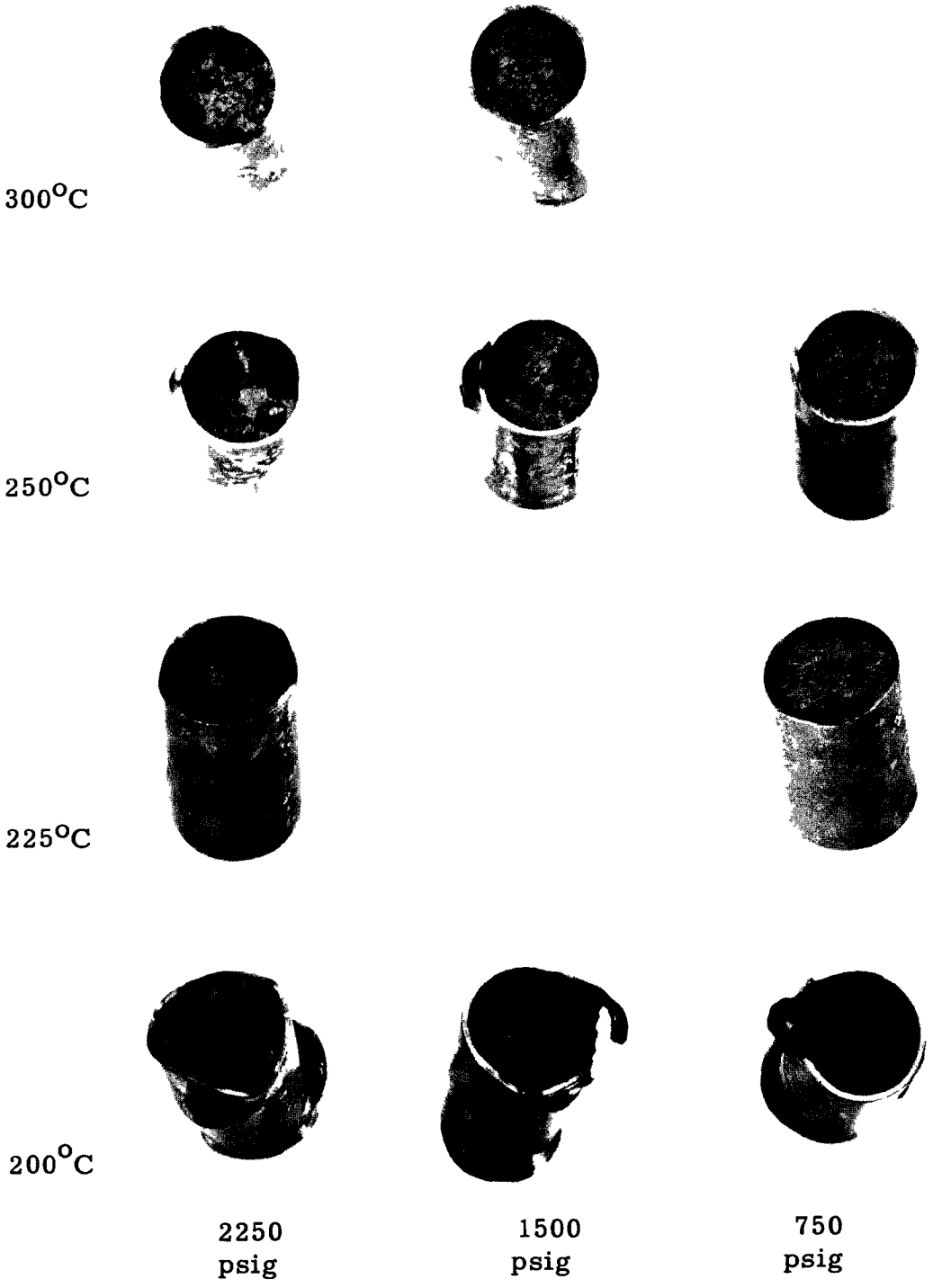

FIGURE 5

Corroded Uranium Samples

AEC GE RICHLAND WASH

The corrosion curves based on hydrogen collection data are shown in Figures 6 through 9. The broken lines are the linear corrosion curves that would be predicted from the uniform oxidation rates. Since the measured uniform penetrations are in such good agreement with the linear oxidation rates of the literature, it was concluded that the samples must have corroded at least as fast as indicated by the broken lines. The curves based on the hydrogen collection are initially below the broken line, suggesting that during the initial part of the reaction all of the hydrogen was not released. The over-all corrosion curves are probably more truly represented in Figure 10, where the linear uniform oxidation rates are observed initially followed by acceleration due to the nonuniform attack. It is interesting to note that the curves become flatter with decreasing pressure and that for a given pressure the accelerated rate is relatively insensitive to temperature.

Nature of the Nonuniform Attack

The question arose as to the specific nature and cause of the nonuniform attack which is so predominant and destructive at 200 C. To determine whether the presence of the Zircaloy cladding caused the nonuniform attack, two unclad cylinders of uranium were exposed at 200 C and 300 C with the results shown in Figure 11. The nonuniform attack was still present on the ends of the 200 C sample. A bare uranium sphere was exposed at 200 C to determine whether the sample geometry contributed to the attack. As seen in Figure 12, the sphere was attacked at two opposite poles which corresponded to the ends of the rolled rod from which it was machined. In other words the nonuniform attack was a function of exposure temperature, and penetration occurred in the direction of extrusion (in the case of the cylinders) and the direction of rolling (in the case of the sphere).

The following observations were made on the nonuniform attack:

1. The presence of the cladding and the sample geometry have no effect.
2. The attack penetrates into the working direction of the uranium, possibly along stringers.
3. The extent of the attack increases with increased pressure. The maximum attack is observed at 200 C.

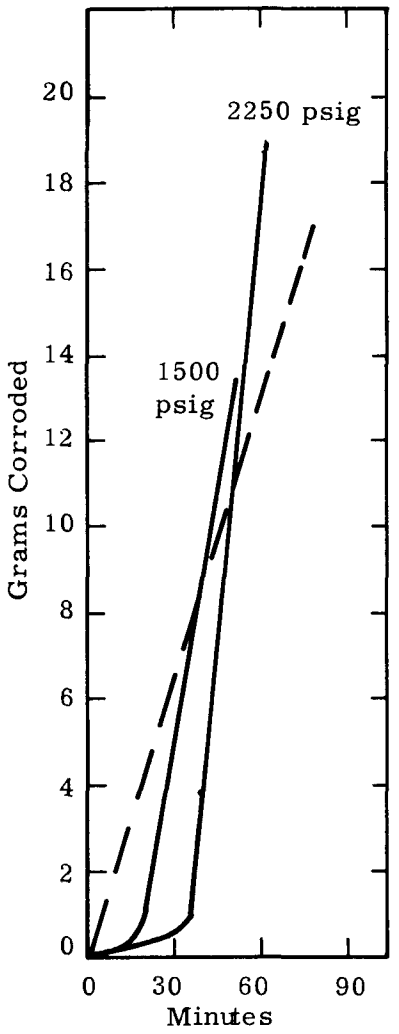

FIGURE 6

Corrosion at 300 C

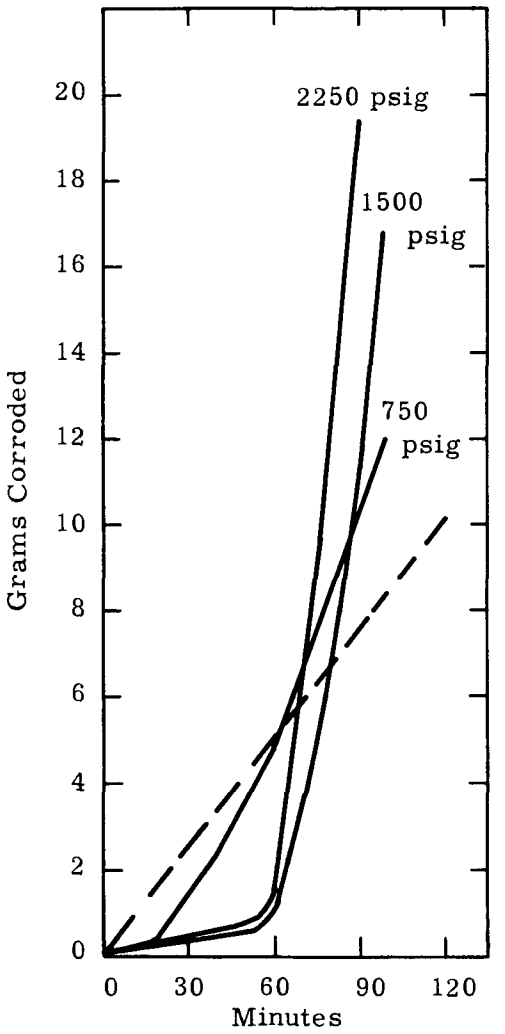

FIGURE 7

Corrosion at 250 C

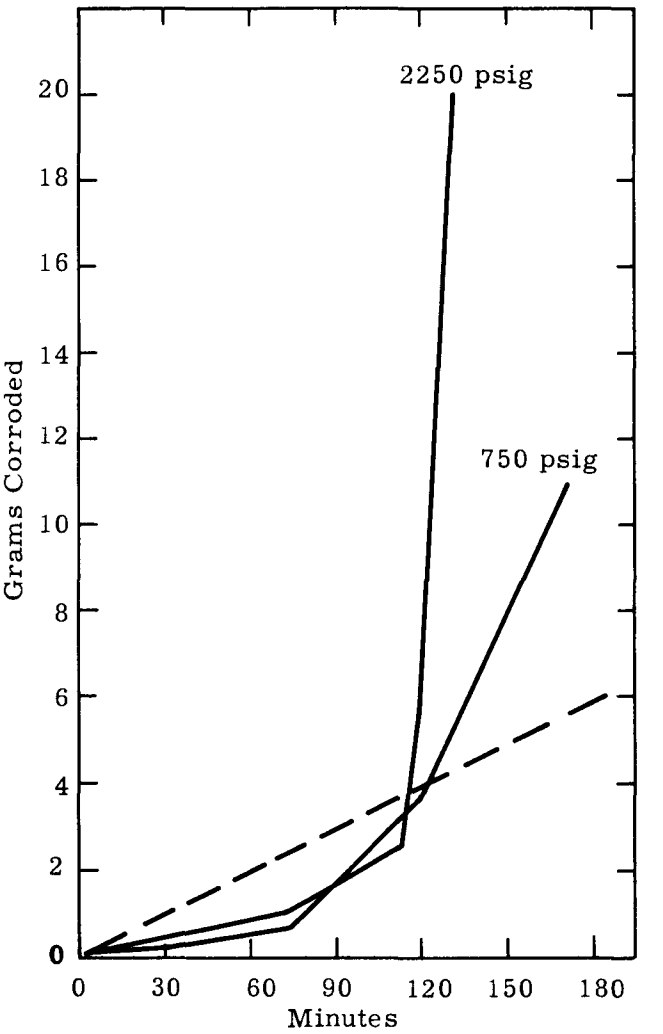

FIGURE 8

Corrosion at 200 C

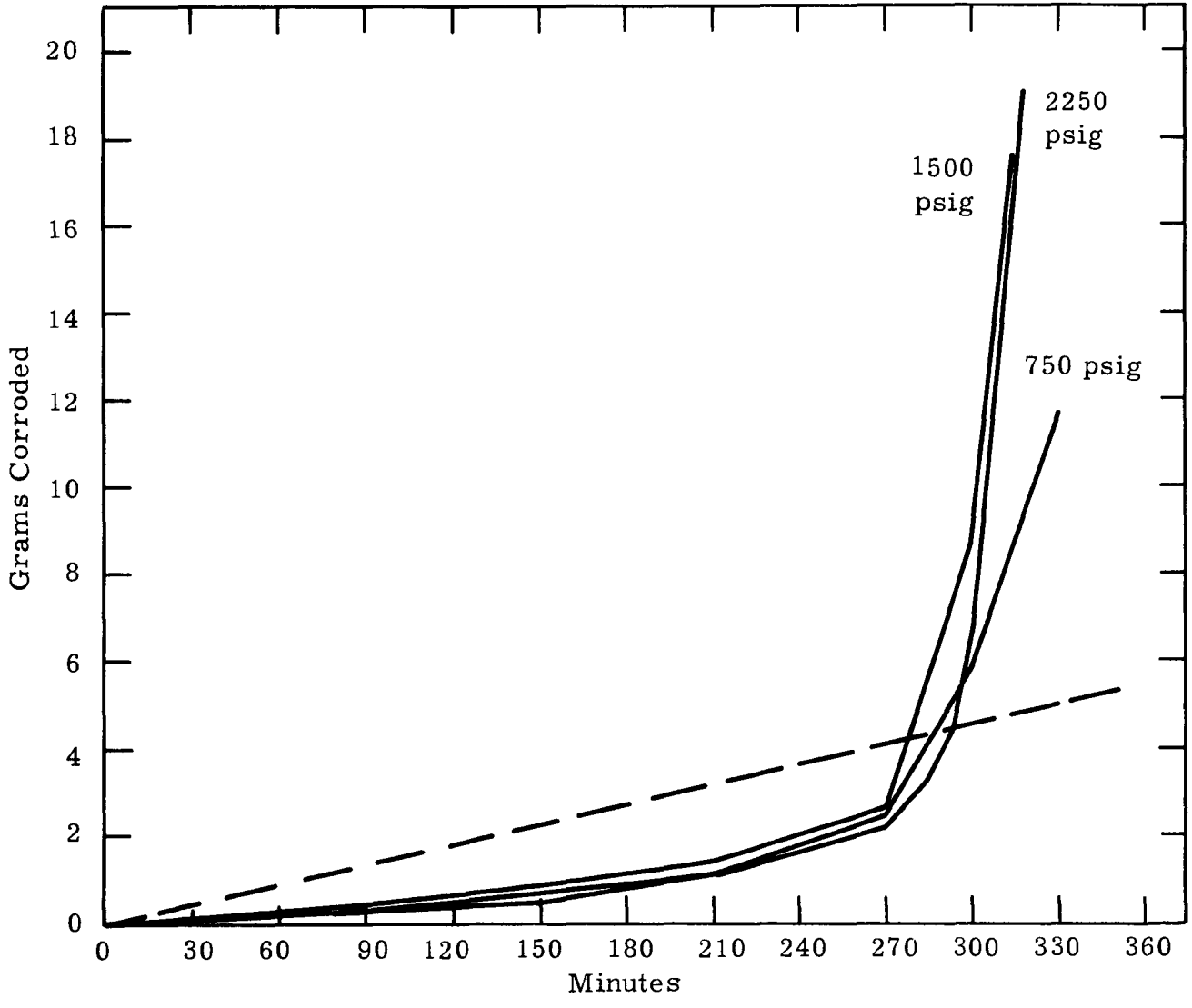

FIGURE 9

Corrosion at 200 C

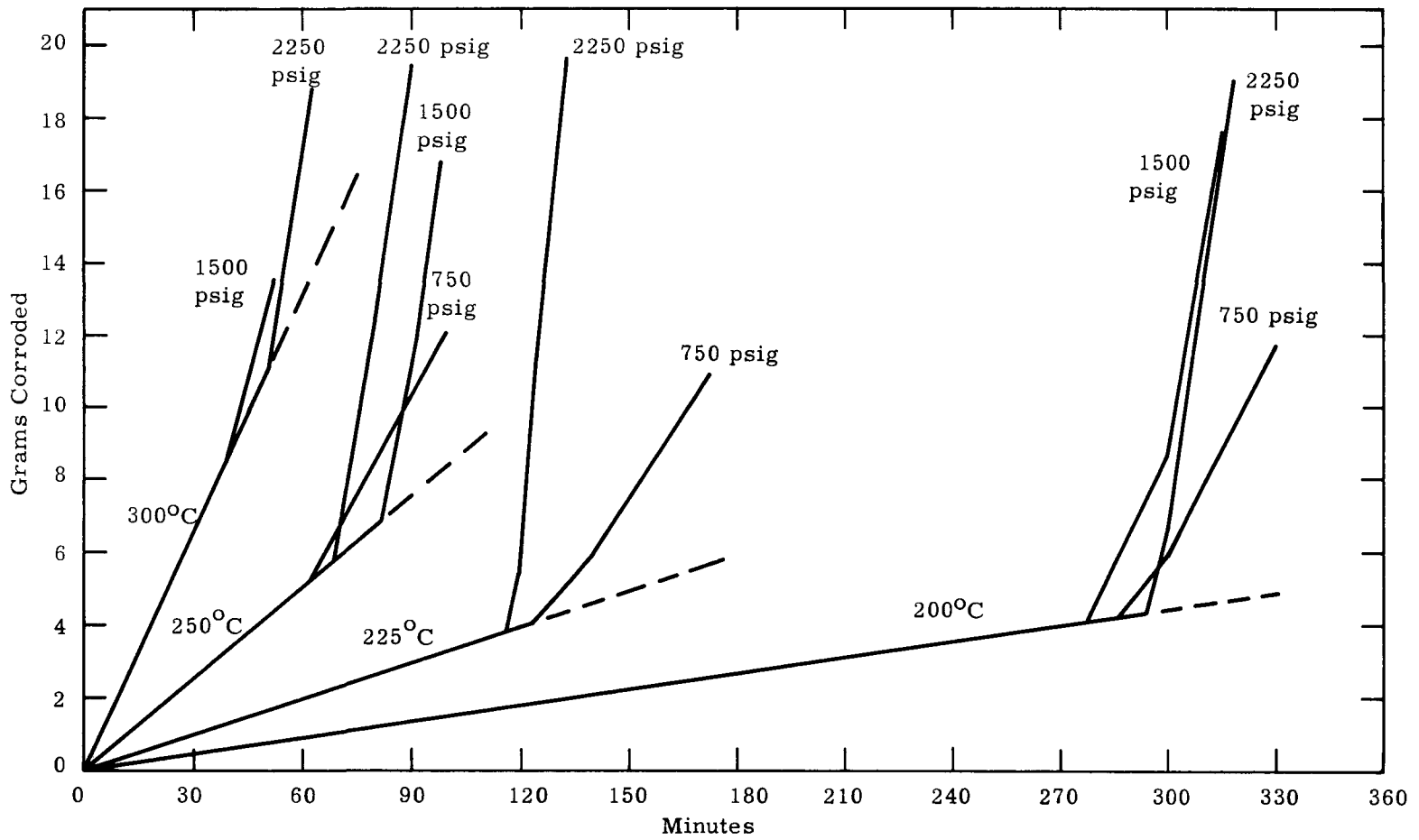

FIGURE 10

Summary of Corrosion Curves

200 C
1500 psig

300 C
1500 psig

FIGURE 11

Corroded Bare Cylinders of Uranium

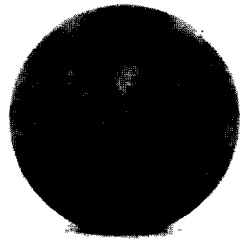

200 C
1500 psig

FIGURE 12

Corroded Uranium Sphere

AEC-GE RICHLAND, WASH.

4. As previously mentioned, not all of the corrosion product hydrogen is released during the initial period.

It was concluded that the nonuniform attack was caused by the penetration of hydrogen into the metal along stringers of inclusions (probably carbide) with the formation of uranium hydride within the metal. Expansion due to hydride formation disrupts the metal which eventually permits the entrance of water and the conversion of the hydride to oxide.

To demonstrate that the nonuniform penetration was along carbide stringers, samples of low carbon dingot uranium (30 ppm carbon) were exposed at 200 C. The nonuniform attack was eliminated.

The nature of the nonuniform attack is verified by the micrographs of Figures 13 and 14. They are cross-section micrographs showing the junction of the uranium and Zircaloy cladding of corroded open-end samples. Figure 13 is typical of samples exposed above 250 C and the low carbon sample exposed at 200 C. The attack is uniform and there is no evidence of hydriding of the uranium or Zircaloy. It is quite probable that a thin layer of UH_3 existed on the uranium surface during exposure but this would be rapidly removed by the water or the post-exposure cleaning. The sample shown is, in fact, the low carbon sample and the absence of carbon inclusions is notable.

Figure 14 shows a sample of ingot uranium (300 ppm C) after exposure at 200 C. Note the presence of carbide stringers. The sample was deeply pitted and these pits contained UO_2, UH_3, and particles of uranium metal. A zone of UH_3 is seen on the surface of the uranium indicating the corrosion proceeds by a hydride front when water is restricted from the reaction site. It is interesting to note the zone of zirconium hydride formed on the inner surface of the cladding, extending to just ahead of the reaction site. This is additional evidence for the inward penetration of hydrogen and the general absence of water at the reaction front.

Effect of Carbon Content

The results obtained with uranium containing from 29 to 1675 ppm carbon, corroded at 300 C and 200 C, are shown in Figures 15 and 16, and in Table II. Corrosion curves, based on corrosion product hydrogen collection, are given in Figures 17 and 18.

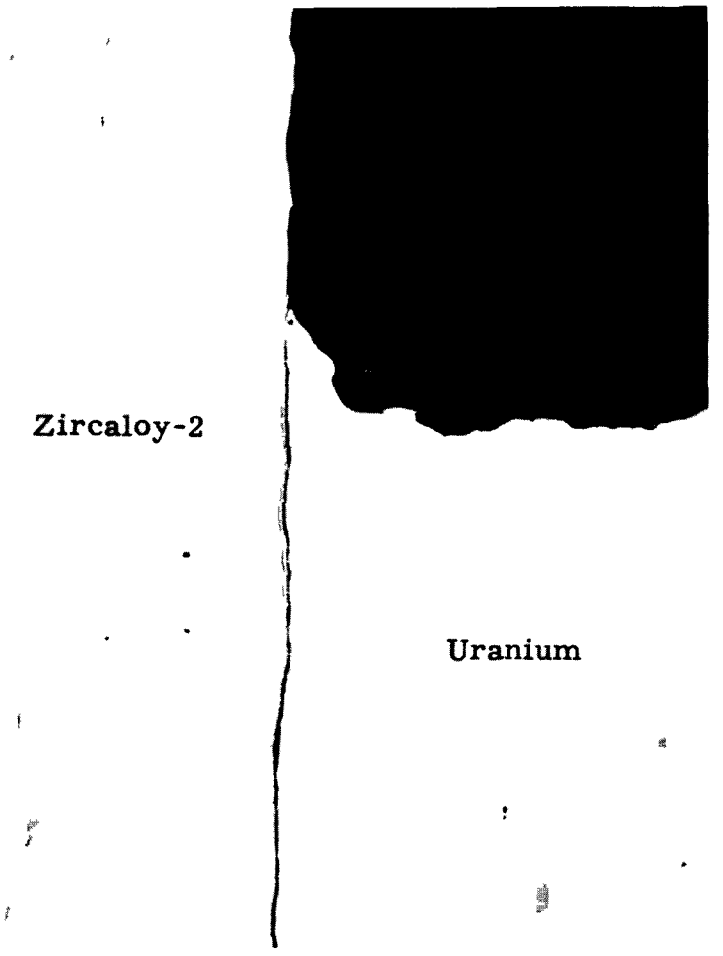

FIGURE 13

Typical Metallograph of Low and High Carbon Samples Corroded at 300 C, and Low Carbon Sample Corroded at 200 C. 250X

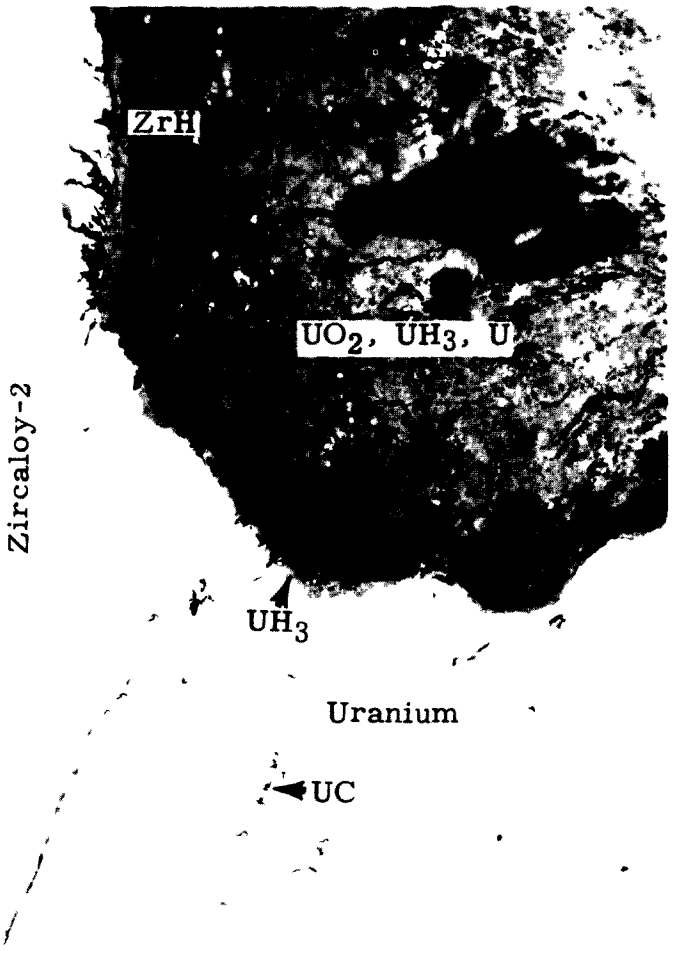

FIGURE 14

High Carbon (300 ppm) Sample Corroded at 200 C 250X

A. 29 ppm C B. 62 ppm C C. 396 ppm C D. 1675 ppm C

FIGURE 15

Corrosion Samples at 300 C, 1500 psig

A. 29 ppm C B. 62 ppm C C. 396 ppm C D. 1675 ppm C

FIGURE 16

Corrosion Samples at 200 C, 1500 psig

TABLE II

EFFECT OF CARBON CONTENT ON URANIUM CORROSION

Test Conditions	Carbon Content	Weight Loss	Measured Uniform Penetration	Exposure Time		Uniform Penetration Rate	Attack
	(ppm)	(g)	(mils)	(min)			
300 C	29	16.8	108	75		1.44	uniform
1500 psig	62	11.0	64.5	47		1.37	"
	396	10.5	67.5	52		1.30	"
	1675	10.1	62.0	44		1.41	"
					Avg.	1.38	
200 C	29	12.7	83.8	702		0.12	uniform
1500 psig	62	17.8	37.4	350		0.11	nonuniform
	396	13.5	31.1	280		0.11	nonuniform
	1675	14.6	*	344		*	nonuniform
					Avg.	0.11	

* Too badly distorted to permit measurement.

At 300 C the attack on all samples was uniform with an apparent average penetration rate of 1.38 mils/minute. Re-evaluation of this rate in terms of an induction period, to be discussed in the next section, gives a penetration rate of 2.0 mils/minute in excellent agreement with the literature rate data.

At 200 C all samples containing more than 29 ppm C suffered severe nonuniform penetration. The uniform rates, as measured from the cladding edge to the flat uranium areas, were 0.11 mils/minute in excellent agreement with literature data. In spite of this rather low penetration rate, the over-all rate based on hydrogen collection became quite rapid as seen in Figure 18. This acceleration of the over-all rate is undoubtedly due to increased corroding surface area resulting from the nonuniform hydride penetration of the uranium.

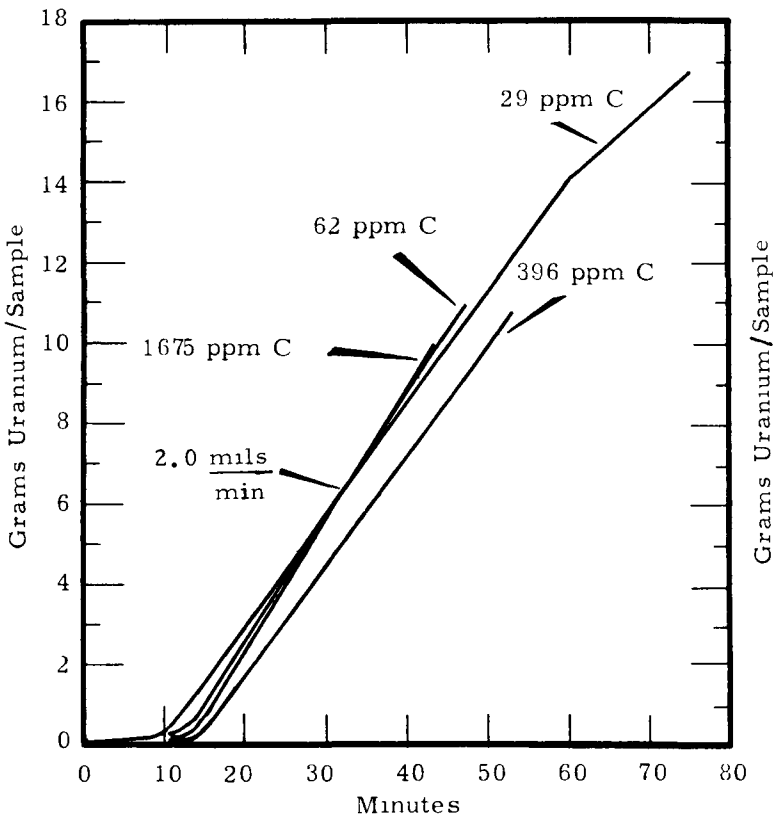

FIGURE 17

Effect of Carbon Content on Corrosion at 300 C, 1500 psig

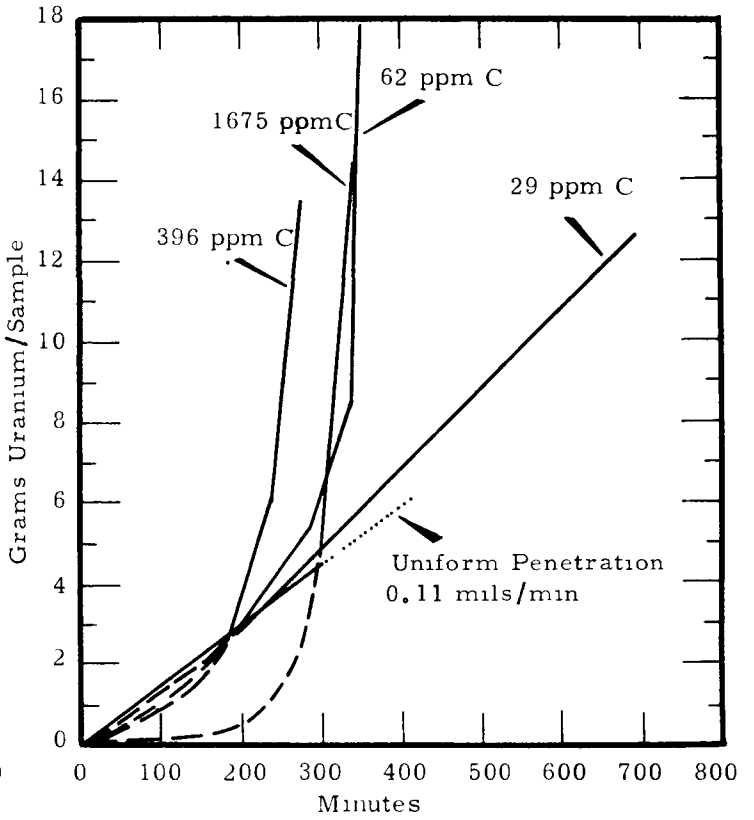

FIGURE 18

Effect of Carbon Content on Corrosion at 200 C, 1500 psig

Induction Period

The uniform penetration rates measured at 300 C, 1500 psig, range from 1. 38 to 1. 59 mils/minute (see Tables I and II). The rate predicted from the literature data in Figure 1 is 2. 0 mils/minute which is somewhat higher than the rates observed. Since there was little or no pitting at 300 C, the apparent acceleration of corrosion shown by the curves in Figure 17 is perplexing. If the uniform linear penetration is preceded by a 10 to 15 minute induction period, then the curves of Figure 17 would truly show the course of corrosion. That is, a 10 to 15 minute induction period with very little corrosion followed by a high linear corrosion rate. The penetration rate calculated from the curves after 15 minutes is 2. 0 mils/minute, in excellent agreement with the predicted value.

At 200 C the measured uniform penetration rates, assuming they are linear through the origin, are in agreement with prediction. This probably means that the induction period at 200 C is too short to be noticeable. This would be true if the induction period was no longer than 10 to 20 minutes.

It was assumed, therefore, that there is an induction period of 10 to 15 minutes prior to corrosion at 300 C and an induction period of about the same duration at 200 C. Therefore, the linear uniform corrosion rates should be evaluated from the curves after the apparent induction period.

Effects of Zirconium Additions to Uranium

Open-end corrosion samples of uranium containing from 0. 12 per cent to 2. 01 per cent zirconium were corroded at 300 C and 200 C. The results are shown in Figures 19 and 20 and in Table III. The hydrogen based corrosion curves are shown in Figures 21 and 22.

At 300 C the corrosion was uniform in all cases. It is apparent from Figure 21 that there was an induction period of 10 to 20 minutes. The addition of zirconium reduced corrosion rates. The greatest reduction was with the 1. 6 per cent zirconium alloy which corroded at a rate of less than one third that of unalloyed uranium. The addition of small amounts of zirconium (0. 12 to 0. 38 per cent) have little effect on the corrosion rate.

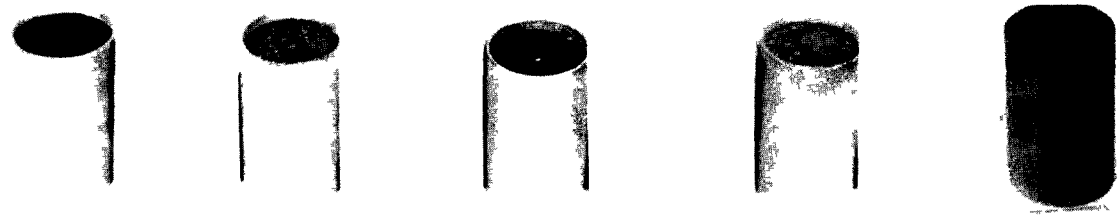

A. 2.01% Zr 40 ppm C | B. 1.65% Zr 1100 ppm C | C. 1.00% Zr 40 ppm C | D. 0.38% Zr 400 ppm C | E. 0.12% Zr 80 ppm C

FIGURE 19

Corrosion Samples at 300 C, 1500 psig

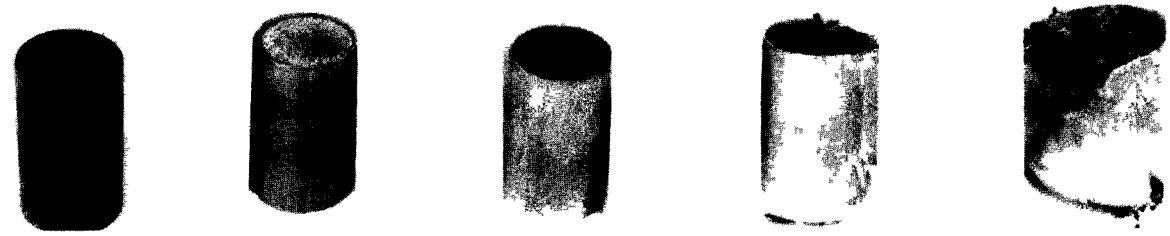

A. 2.01% Zr 40 ppm C | B. 1.65% Zr 1100 ppm C | C. 1.00% Zr 40 ppm C | D. 0.38% Zr 400 ppm C | E. 0.12% Zr 80 ppm C

FIGURE 20

Corrosion Samples at 200 C, 1500 psig

TABLE III

EFFECTS OF ZIRCONIUM ADDITIONS

Test Conditions	Zirconium Content (Per Cent)	Carbon Content (ppm)	Uniform Penetration (mils)	Exposure Time (min)	Induction Time (min)	Penetration Rate (mils/min)	Attack
300 C	0	29	108	75	10	1.66	uniform
1500 psig	0.12	80	73.0	65	17	1.52	uniform
	0.38	400	61.0	48	11	1.65	uniform
	1.00	40	69.5	102	20	0.85	uniform
	1.65	1100	64.0	95	20	0.85	uniform
	2.01	40	73.5	77	15	1.19	uniform
	1.6*	200	47.0	96	20	0.62	uniform
200 C	0	29	83.8	702		0.12	uniform
1500 psig	0.12	80	**	343		**	nonuniform
	0.38	400	34.8	335		0.103	nonuniform
	1.00	40	16.0	480		0.033	uniform
	1.65	1100	16.0	462		0.034	uniform
	2.01	40	36.0	817		0.044	uniform
	1.6*	200	5.0	380		0.013	uniform

* Material fabricated at NMI with nominal 2 per cent zirconium content. HAPO analysis showed it to be 1.6 per cent zirconium.

** Too badly distorted to permit measurement.

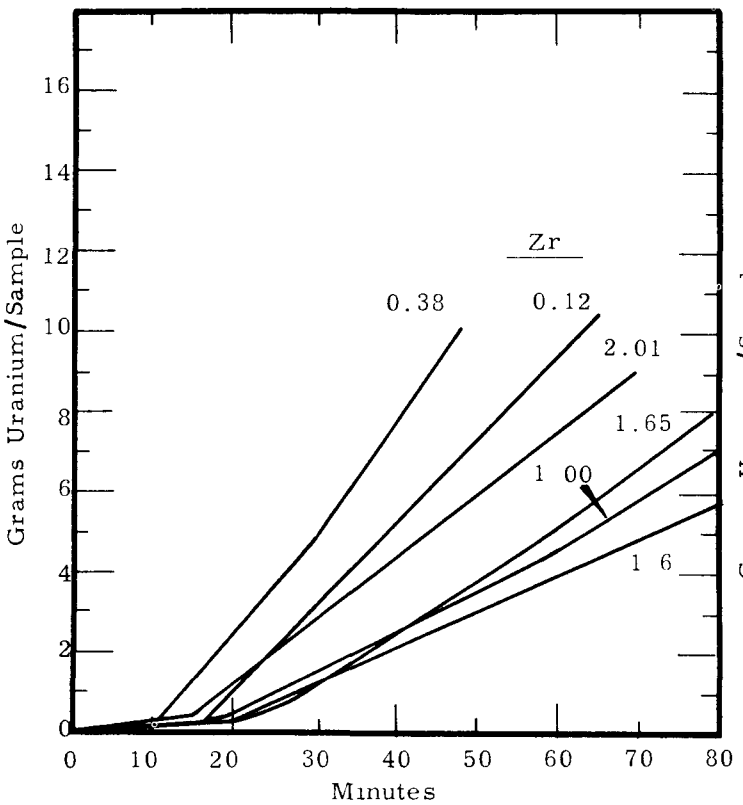

FIGURE 21

Effect of Zirconium Content on Corrosion at 300 C, 1500 psig

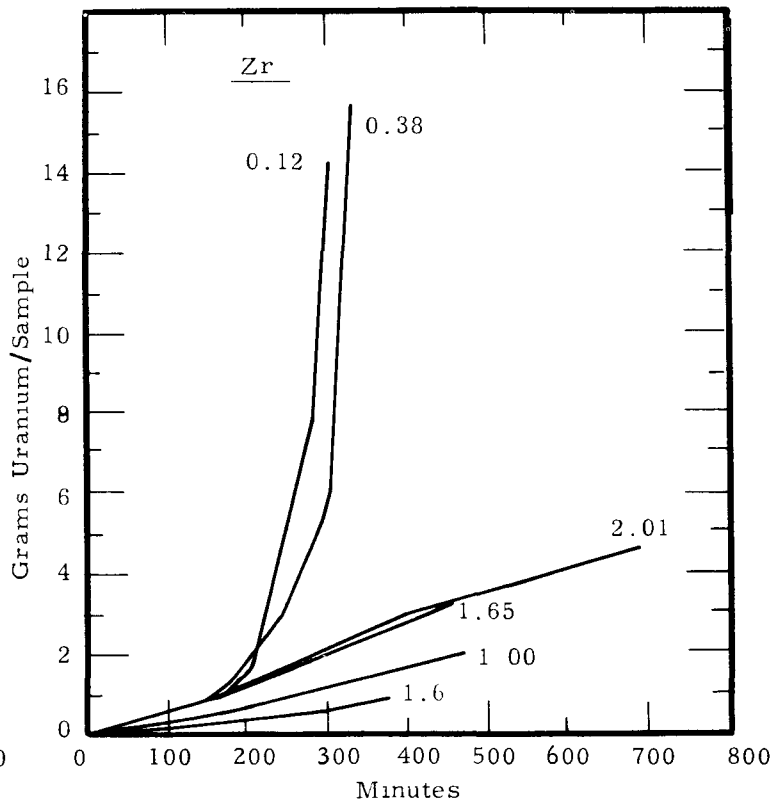

FIGURE 22

Effect of Zirconium Content on Corrosion at 200 C, 1500 psig

At 200 C the corrosion was nonuniform for the low zirconium additions (0. 12 and 0. 38 per cent), resulting in accelerating attack. Material containing 1 per cent or more zirconium showed only uniform corrosion in spite of carbon contents as high as 1100 ppm. The 1. 6 per cent alloy showed the greatest reduction in corrosion rate; about one seventh that of unalloyed uranium.

The temperature dependence of uranium-zirconium alloy corrosion is shown in Figure 23.

Effects of Heat Treatment

Open-end samples were corroded at 300 C with the following prior heat treatments:

1. As-extruded
2. β treated - water quenched
3. β treated - air cooled
4. β treated - furnace cooled
5. β treated - interrupted quench (cooled to 590-600 C, held for 10 minutes then air-cooled).

Beta treatment consisted of 10 minutes at 720 to 730 C.

There was no significant difference in corrosion rates for these samples. All the samples corroded uniformly.

Effects of Irradiation

No experimental work was performed on the effects of irradiation on uranium corrosion in connection with this program. Indeed, there is very little information available in the literature. A test conducted at Argonne National Laboratory[17] has shown no appreciable effect of irradiation on the aqueous corrosion of uranium. In boiling water at 100 C, uranium irradiated to 0. 1 atom per cent burnup had a corrosion rate of 75 $mg/cm^2/day$ as compared to about 70 $mg/cm^2/day$ for unirradiated uranium. This is the same value as that obtained at Battelle[5] for unirradiated uranium at 100 C.

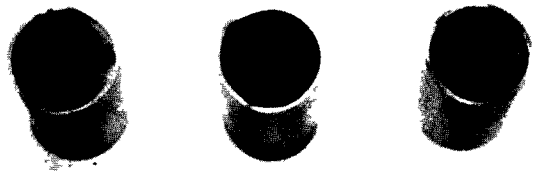

1 2 3

1. 500 C, 2000 psig
2. 500 C, 1000 psig
3. 500 C, 200 psig

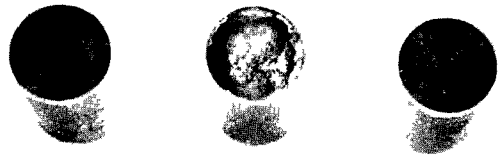

4 5 6

4. 400 C, 2000 psig
5. 400 C, 1000 psig
6. 400 C, 200 psig

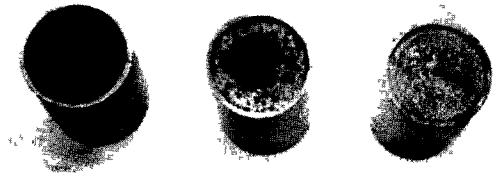

7 8 9

7. 300 C, 1000 psig
8. 300 C, 200 psig
9. 225 C, 200 psig

FIGURE 23

Samples Corroded in Steam

AEC GE RICHLAND, WASH

Corrosion of Uranium in Steam

Open-end samples of ingot uranium were exposed to steam at 225 C to 500 C at pressures from 200 to 2000 psig. The samples are shown after exposure in Figure 23. The results are given in Table IV and the corrosion curves, based on hydrogen collection, are shown in Figure 24.

The samples underwent two kinds of attack, uniform penetration, and in some cases, the formation of a deep cavity. In most cases where the deep cavity form of attack was present, flat plateau areas were still present which permitted measurement of a uniform penetration rate. The two types of results obtained are shown in Figure 4A and 4C.

As shown in Table IV, the uniform penetration rate increases with increasing temperature and pressure, although the rates at 500 C are lower than those at 400 C. Uniform rates in steam are somewhat less than those in water at the same temperature, probably due to the lower pressure. For comparison the penetration rates in water are 0. 25 mils/minute at 225 C, and 2. 0 mils/minute at 300 C (see Figure 10).

The solid curves in Figure 24 show the total corrosion based on hydrogen collection during the test. The borken lines represent the uniform corrosion rates (assumed linear) corresponding to the measured uniform penetrations. The positive deviation (or acceleration) of the total corrosion rate from the linear uniform rate corresponds to the extent of the cavity attacks. The tendency toward cavity attack increases with increasing temperature and pressure. Sample 9 (225 C, 200 psig) shows no cavity attack and its corrosion curve coincides with the linear uniform penetration rate. Samples 6 and 7 (400 C, 200 psig, and 300 C, 1000 psig) show only slight cavity attack and their corrosion curves are linear and just slightly higher than the uniform penentration curves. These three samples confirm the assumption that in the absence of cavity attack the corrosion is uniform and linear with time. Samples 3 and 8 (500 C, 200 psig, and 300 C, 200 psig) show moderate cavity attack and their corrosion curves show moderate acceleration above the linear uniform rates. The four remaining samples (400 C, 500 C, and 1000 psig, 2000 psig) show severe cavity attack and their corrosion curves are greatly accelerated.

TABLE IV

STEAM CORROSION OF URANIUM

Sample	Temperature (C)	Pressure (psig)	Time (min)	Uniform Penetration (mils)	Penetration Rate (mils/min)	Uniform Penetration Rate (g/min)	Total Weight Loss (g)	Extent of Cavity Attack
1	500	2000	10.5	18	1.7	0.27	30	Severe
2	500	1000	13	13	1.0	0.16	21	Severe
3	500	200	38	30	0.79	0.12	9.6	Moderate
4	400	2000	10.5	22	2.1	0.33	20	Severe
5	400	1000	18	25	1.4	0.22	15	Severe
6	400	200	34	32.5	0.96	0.15	6.5	Slight
7	300	1000	37.5	32.5	0.87	0.14	6.7	Slight
8	300	200	85	41.5	0.49	0.077	14	Moderate
9	225	200	132	22	0.17	0.027	3.8	None

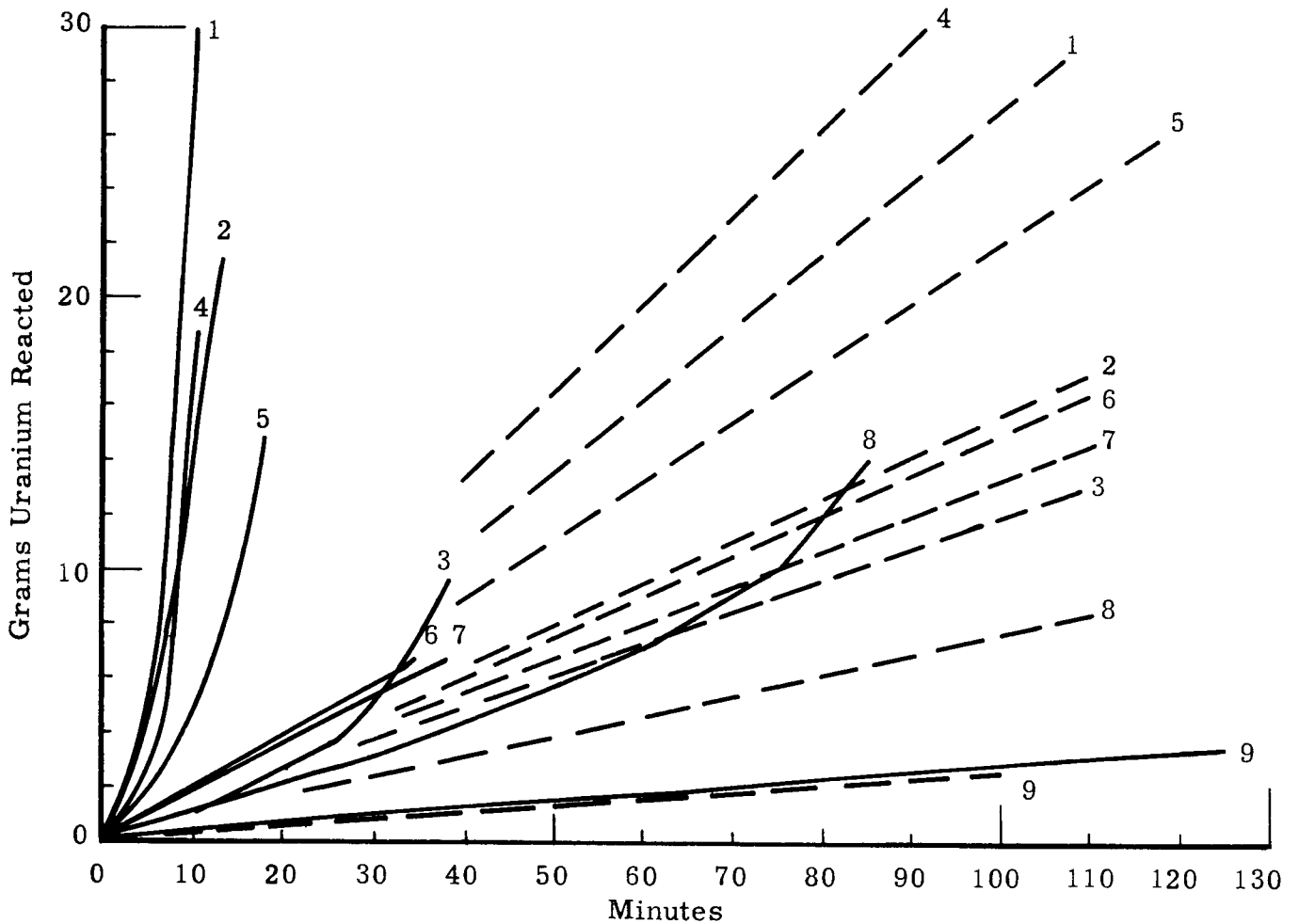

FIGURE 24

Uranium Corrosion in Steam

Nature of Steam Corrosion

It was concluded that the uniform penetration corresponded to the corrosion of uranium at the ambient steam temperature and pressure. The cavity attack is caused by self-heating of the uranium to much higher temperatures due to the heat generated by the corrosion reaction, the poor heat transfer properties of steam, and the insulation by the uranium oxide corrosion product. The nature of the cavity attack was confirmed in an experiment conducted in the direct viewing unit (sight glass). The core of a rupturing fuel element was observed to "burn" at about 700 C in a 310 C, 1000 psig steam atmosphere. This experiment is described more fully in a later section (Rod Elements in Steam).

FUEL ELEMENT RUPTURE BEHAVIOR

Rod Elements in Water

Most of the rod element rupture studies are conducted with samples of the following description:

Dimensions - 0.59 inch OD, 2 inch length.

Core - natural ingot uranium containing about 300 ppm carbon.

Cladding - Zircaloy-2, coextruded, 30 mils thick.

End Closures - Zircaloy-2 caps, welded, unbonded.

Heat Treatment - heat treated at 720 to 730 C for 10 minutes, followed by 10 minutes at 590 to 600 C, and then air cooled.

Defect - 25 mil diameter pinhole drilled through the cladding into the uranium core, and located at the middle of the element.

The heat treatment described is referred to as β treatment followed by an "isothermal" or "interrupted" quench. This heat treatment was selected because preliminary tests indicated that it gave the lowest rupture rates. Heat treatment is discussed more fully in a later section. The 25 mil pinhole defect size was selected for convenience in drilling and because it coincided with the majority of the "defect tests" run elsewhere. The effect of defect size is disussed in a later section.

The basic behavior of a defected fuel element sample in water is shown in Figure 25, along with its rupture curve based on hydrogen collection. This sample was removed at various intervals during exposure at 300 C, 1500 psig. The initial exposure period is called the induction period. During this time a blister forms at the site of the defect. There is no observable release of hydrogen or oxide corrosion product during this period (A, Figure 25). The induction period is terminated by failure of the cladding around the base of the initial blister permitting the first release of corrosion products. Expansion of the core, resulting from its conversion to oxide, forces the blister open, permitting increased water entry to the core (B, Figure 25). Corrosion of the core occurs under the cladding and new blisters form and grow adjacent to the original blister. The rupture proceeds by a succession of blisters and the increased area of exposed core results in rapid acceleration of the rupture rate (C and D, Figure 25). These observations were confirmed by continuous observations of a fuel element sample rupturing in the direct-viewing unit. Under certain conditions the rupture behavior is different, but the behavior described is typical of ruptures in water at 250 C and above.

Rupture curves obtained in water from 170 to 350 C are given in Figure 26 and the induction periods are given in Table V. The induction period decreases with increasing temperature. For a given temperature, increasing pressure reduces the induction period at 200 C, but has little effect at higher temperatures. At 250 C and above, the rupture rates are eventually much the same, although the initial rate of rupture is slower at the lower temperatures. At 200 C the induction period is long and the rate of rupture is somewhat slower. In tests conducted for longer periods of time, the rupture rate at 200 C eventually accelerated to give rates even higher than at 300 C. The sample exposed at 170 C ran for 50 hours with no visible sign of attack. Varying pressure had no consistent effect on the rupture rates and the variations observed at a given temperature are probably an indication of experimental reproducibility.

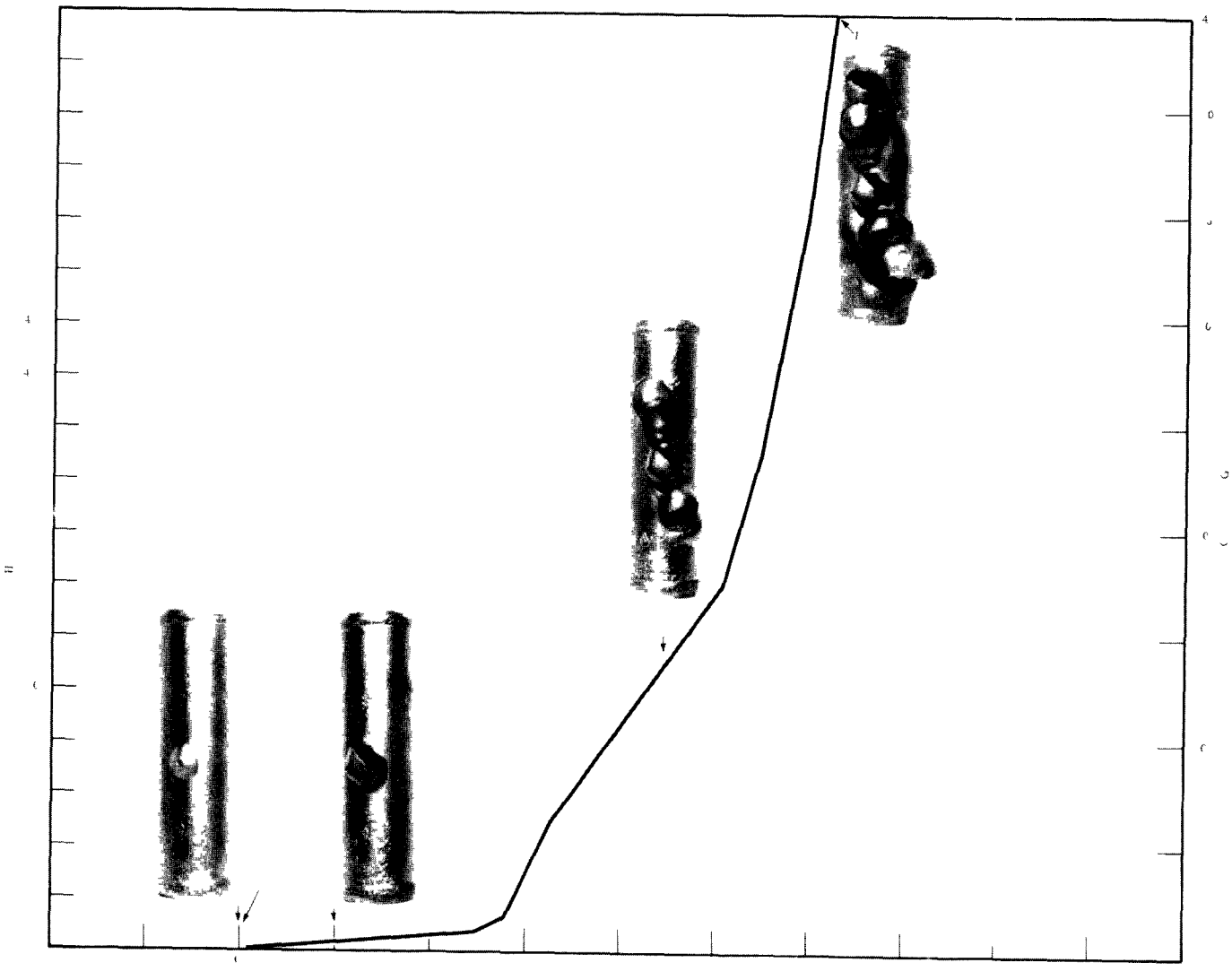

FIGURE 25

Rupture Curve at 300 C, 1500 psig

TABLE V

INDUCTION PERIODS FOR PINHOLE DEFECTED ROD ELEMENTS

Temperature	Pressure	Induction Period
350	2800 psig	0 minutes
300	2500	57
300	2500	54
300	1500	49
300	1500	51
250	1500	100
250	1500	140
200	2500	7 hours, 20 minutes
200	1500	10 hours
200	1500	13 hours
200	500	17 hours, 32 minutes
170	500	Greater than 50 hours

At 200 C the rupture behavior is different than at the higher temperatures. Swelling of the fuel sample occurs over a large area accompanied by tearing of the cladding. The uranium remaining in the sample after testing is extensively penetrated giving a "sponge-like" appearance. By comparison, ruptures at 250 C and above proceed by successive blistering with very little general swelling, and the corroded core has a smooth walled cavity after testing. In a 200 C rupture test conducted in the direct viewing unit, the cladding was observed to hydride some distance from the rupture site, resulting in brittle failure of the cladding even before swelling occurred. A typical 200 C ruptured element is shown in Figure 27B.

Effect of Carbon Content

The extensive swelling and spongy appearance of the uranium, encountered in ruptures at 200 C in water, clearly results from the internal hydride penetration of the uranium as observed in the previously described corrosion tests.

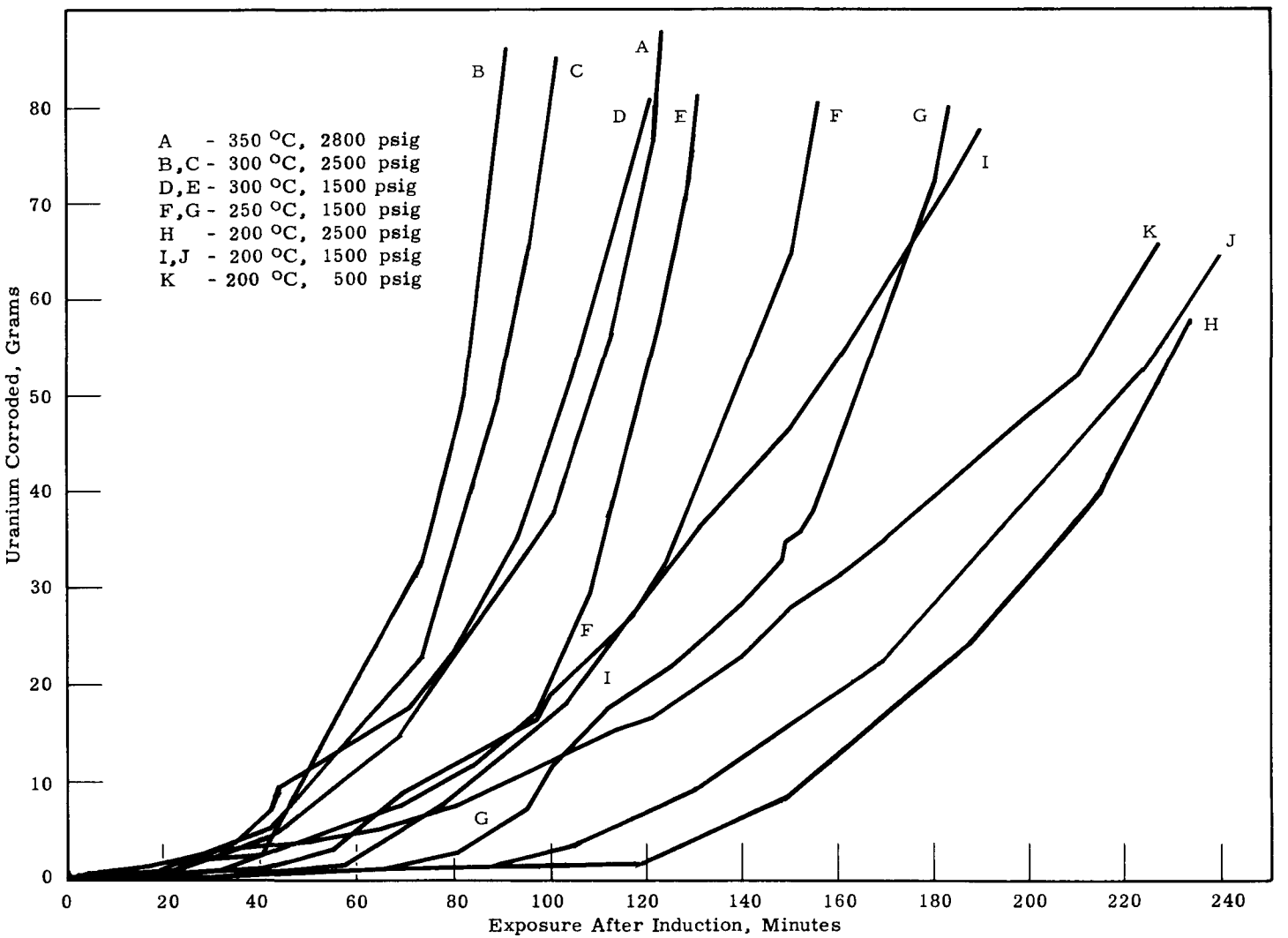

FIGURE 26

Rupture Curves for Pinhole Defected Rod Elements
(β-heat treated, isothermal quench)

A. 200 C
29 ppm C

B. 200 C
300 ppm C

C. 300 C
300 ppm C

FIGURE 27

Ruptured Rod Element Samples

AEC-GE RICHLAND, WASH.

It has been shown that reduction of the carbon content eliminates this nonuniform type of attack on bare uranium. It seemed reasonable to expect that reduction of the carbon content would also eliminate this type of attack in a fuel element rupture. To test this idea, a rod element sample with a dingot uranium core (29 ppm carbon) was ruptured in 200 C water. The result is shown in Figure 27A. While the lengthwise attack was eliminated, severe swelling occurred through the rod at the region of the defect causing the sample to break open. The spongy appearance of the uranium remaining showed that the nonuniform hydride penetration had not been eliminated, but was merely confined to the region near the defect. The rupture curve for this sample is shown in Figure 28 along with the curves obtained for ingot uranium (300 ppm carbon) at 200 C and 300 C. The induction period for the low carbon sample was much longer and the initial rate of rupture was slower. Eventually however, its rupture rate became the same as for the higher carbon sample.

Mechanism of Fuel Rupture and the Carbon Effect

The mechanism which explains the rupture behavior at 250 C and above, and the effect of carbon content at 200 C, is diagramed in Figures 29, 30 and 31.

At 250 C and above the mechanism is as described in Figure 29. Water enters the defect and reacts with the uranium core to form oxide. The oxide blocks the defect and permits only the slow diffusion of water into the core. The hydrogen formed is contained within the cladding where it reacts with the uranium surface to form a layer of uranium hydride (Figure 29A). The reaction proceeds slowly in this fashion until the increased volume of oxide and hydride forms a blister on the cladding which eventually ruptures (generally around the circumference of the blister) permitting the general entrance of water into the core (Figure 29B). The size that the blister attains before the cladding ruptures is a function of bond strength, cladding strength and thickness, and sample diameter, as will be discussed in later sections. Prior to cladding failure, neither hydrogen nor oxide is released from the defect. Water entering the blister reacts with the uranium hydride and uranium core to form oxide and hydrogen which is released. The water continues to react with the

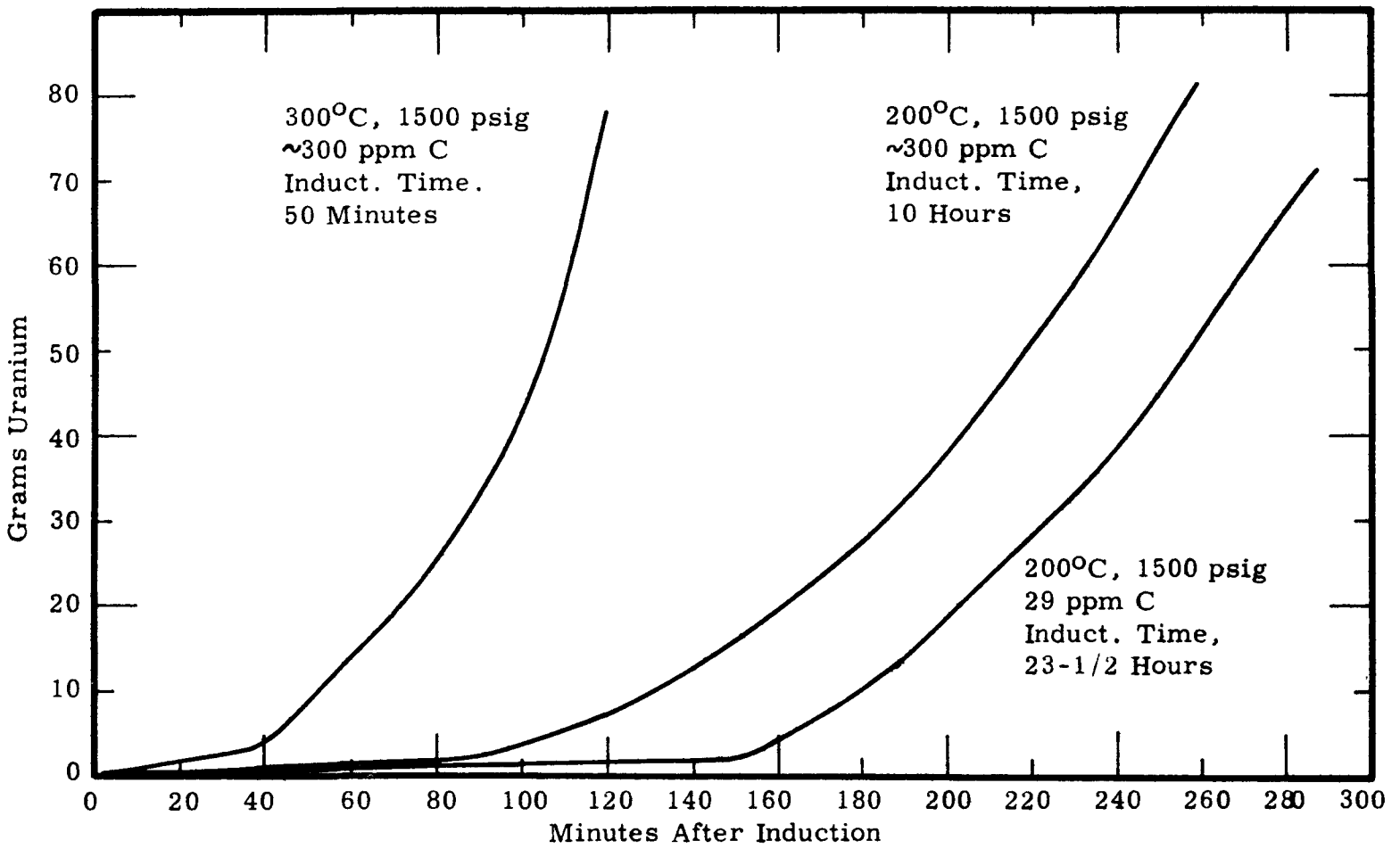

FIGURE 28

Rod Element Rupture Curves - Effect of Carbon Content

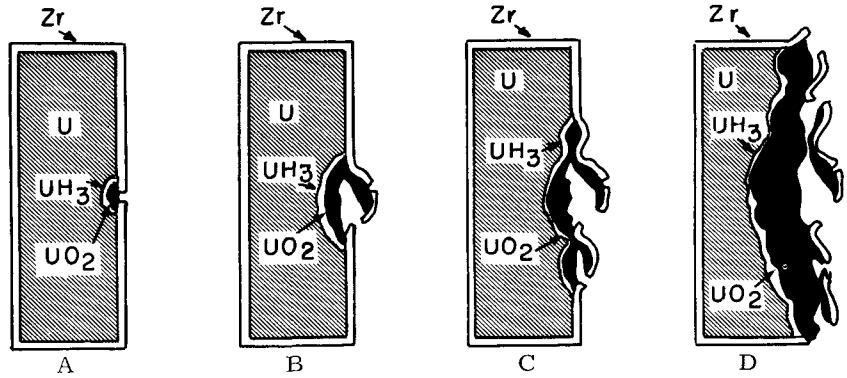

FIGURE 29

Rupture Mechanism at 250 C and Above

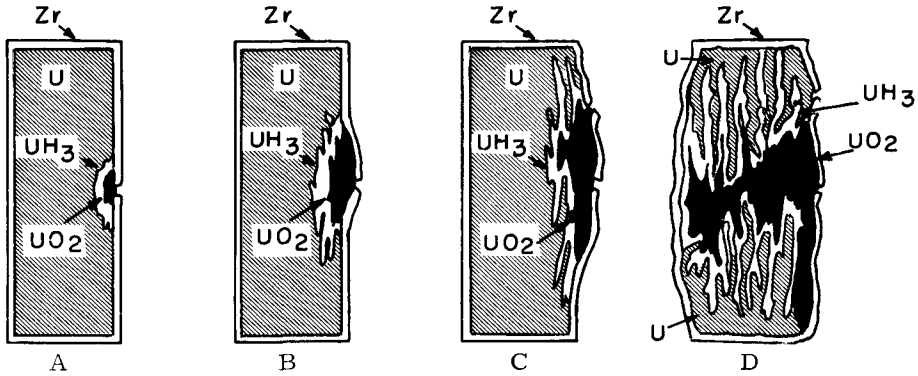

FIGURE 30

High Carbon Rupture Mechanism at 200 C

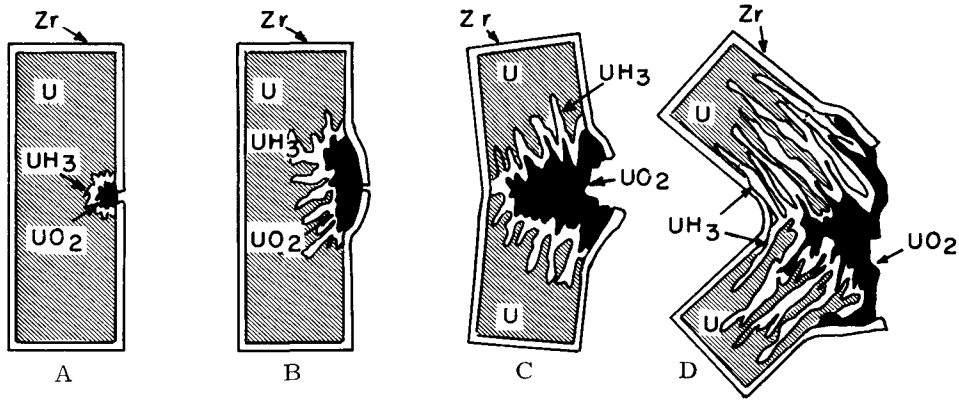

FIGURE 31

Low Carbon Rupture Mechanism at 200 C

uranium core, enlarging the cavity below the blister. Some of the corrosion product hydrogen (probably about 10 per cent, based on material balance calculations) is retained by the uranium as uranium hydride. The hydrogen diffuses more easily down the bond layer than into the uranium core, forming hydride pockets adjacent to the initial blister. This initiates new blisters and, as they grow, water enters and oxidation proceeds until the blisters rupture (Figure 29C). The rupture proceeds in this manner forming a succession of blisters along the bond layer while corroding at a slower rate into the core material (Figure 29D). The increase in corroding surface area, caused by blistering of the cladding, results in an accelerating rate of rupture.

High carbon (ingot) elements at 200 C rupture in the manner shown in Figure 30. Water enters the defect and reacts with the uranium core to form oxide and hydrogen. The oxide blocks the defect, permitting only limited diffusion of water into the core. The hydrogen reacts rapidly with the uranium, forming uranium hydride (Figure 30A). As the reaction proceeds slowly, the increasing volume of uranium oxide and uranium hydride causes a swelling of the cladding. Because the hydride penetrates into the uranium, the swelling of the cladding is spread out over a wide area rather than in a small blister (Figure 30B). As the swelling of the cladding increases, it eventually fails (frequently as a lengthwise split). Carbide stringers in the uranium provide an easy path for diffusion of hydrogen and formation of uranium hydride. Consequently, the hydriding proceeds faster along the length of the fuel element than through the core (Figure 30C). The swelling and tearing of the cladding also proceeds lengthwise. Because the hydriding occurs quite a distance from the point of water entrance, the Zircaloy cladding is also hydrided. The rupture proceeds rapidly after the failure of the cladding because of the rapidity of the hydride reaction and the greatly extended surface area thus exposed (Figure 30D).

Low carbon (dingot) elements at 200 C rupture in the manner shown in Figure 31. The initial stages are similar to those described in the preceding case (Figure 31 A and B). However, because of the absence of uranium carbide stringers, the hydriding reaction is somewhat slower and it proceeds

transversely through the core as fast as it does lengthwise (Figure 31C). The swelling of the cladding extends over a lesser area and severe longitudinal stresses are caused by the wedge-like hydride attack. This results in transverse breaking and distortion of the fuel element (Figure 31D).

Effect of Cladding Thickness

To ascertain the effect of cladding thickness on the behavior of a rupturing element, a rod element sample was turned down to give a 10 mil cladding thickness prior to exposure in 300 C water. The sample and its rupture curve is compared to a 30 mil clad sample in Figure 32. The thin cladding failed when the blisters were still quite small. Consequently, the induction period was shorter and the damage to the cladding less extensive. Rapid failure of the cladding at blisters permitted easy access of water to the core and thus inhibited the hydride attack down the bond layer. As a result, the rate of rupture of the thin clad sample was much slower than the thicker clad sample.

Tests run with 15, 20, and 25 mil cladding gave intermediate results.

Effect of Heat Treatment

An extensive series of tests were run to determine the effects of various heat treatments prior to exposure on the rupture behavior of coextruded fuel element samples. This work was done in cooperation with J. W. Goffard of the Fuel Element Design Operation of Hanford Laboratories. Only the general effects will be discussed here; for more detailed explanation of the effects of heat treatment, reference should be made to Goffard's report.[18]

Rupture curves for samples given various heat treatments prior to exposure at 300 C, 1500 psig, are given in Figure 33. Samples after rupture are shown in Figure 34. Water quenching after β heat treatment (10 minutes at 720-730 C) gives a more rapid rupture than the as-extruded condition. Various slow cooling quench cycles after β treatment were tried which reduced the rate of rupture markedly. The interrupted or "isothermal" quench, and oil quench are shown as examples. It was later found that annealing after water quenching also reduced the rate of rupture. The example shown is a water-quenched sample which was annealed at 400 C for 48 hours. Its

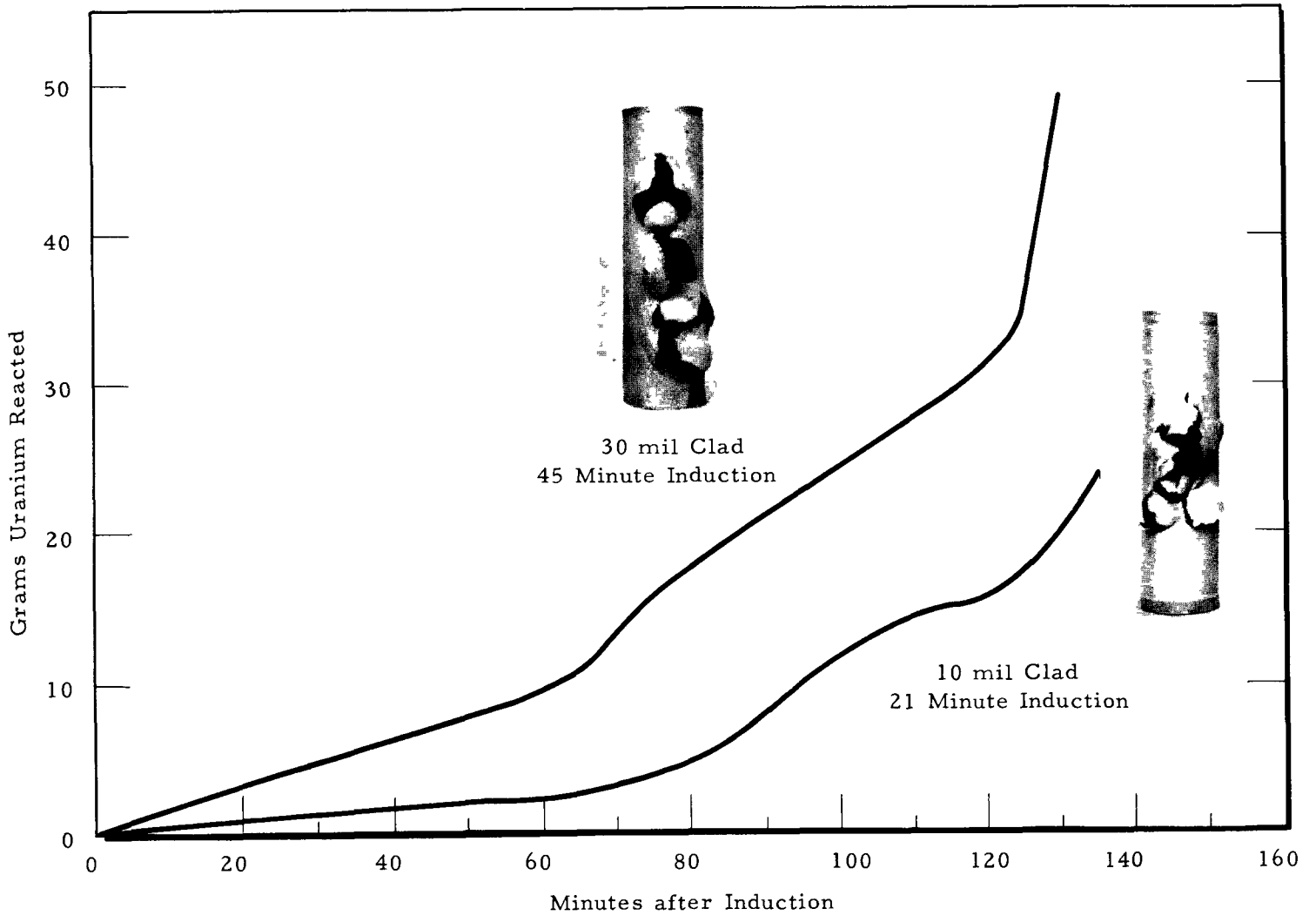

FIGURE 32

Effect of Cladding Thickness

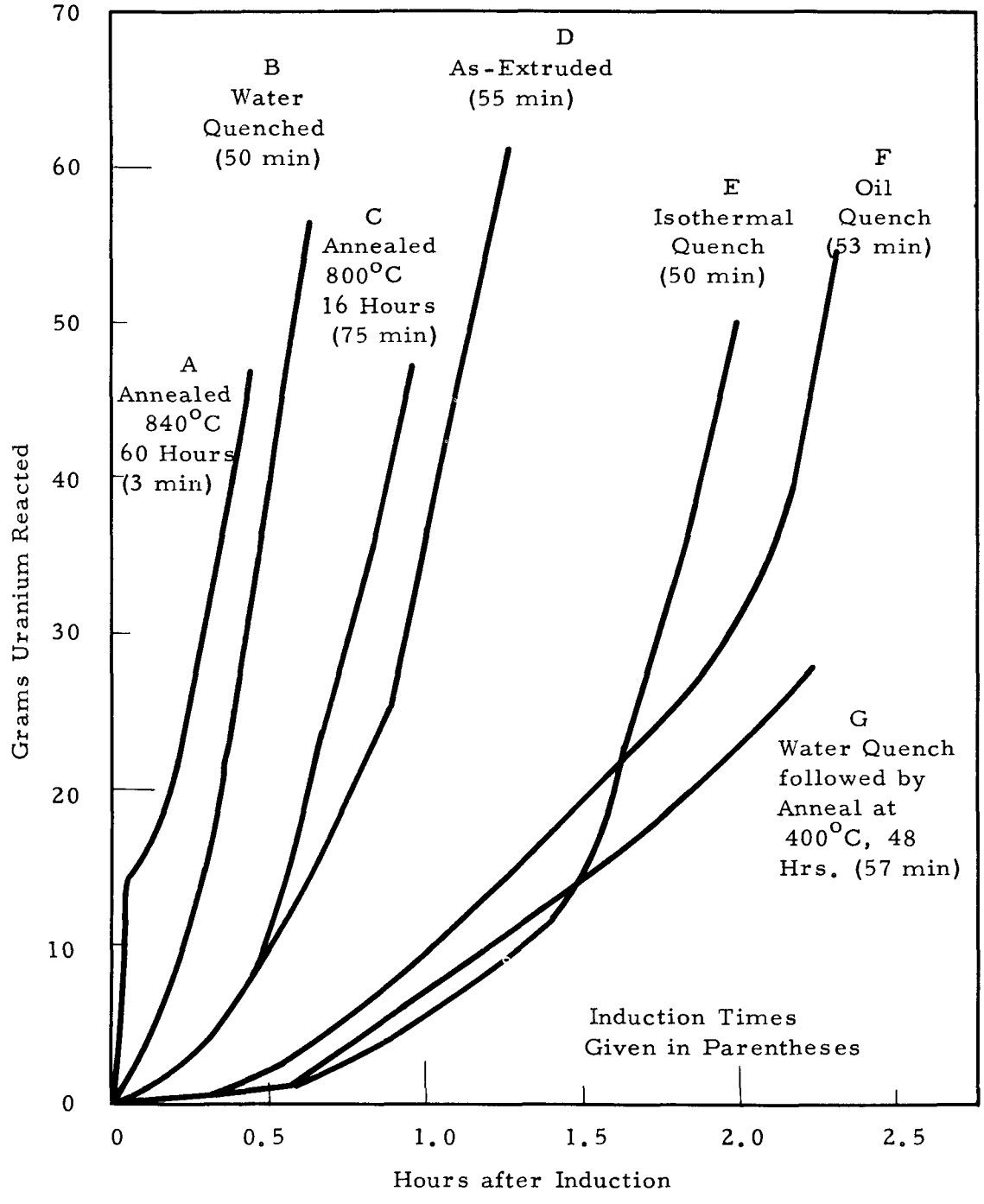

FIGURE 33

Effects of Heat Treatment on Rod Ruptures
at 300 C, 1500 psig

AEC-GE RICHLAND, WASH.

A. Annealed 840 C, 60 Hours

B. Water Quenched

C. Annealed 800 C, 16 Hours

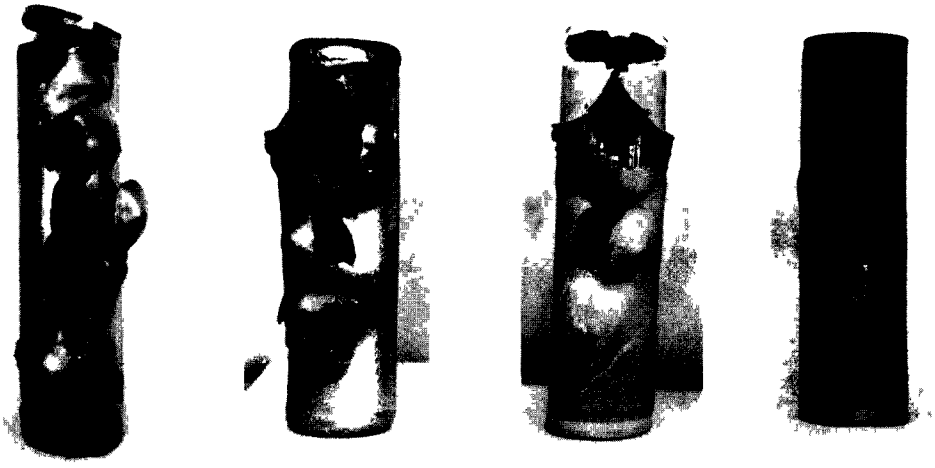

D. As-Extruded

E. Isothermal Quench

F. Oil Quench

G. Water Quench followed by Anneal at 400 C, 48 Hours

FIGURE 34

Rod Elements Ruptured at 300 C, 1500 psig, after Various Heat Treatments

rupture rate was comparable to the slow quenches. The particular significance of this annealing cycle is that this is similar to the heat treatment which a fuel element receives during autoclave "proof-testing" in 400 C steam prior to reactor exposure. The conclusion is that heat treatment during "proof-testing" eliminates the need for the more elaborate slow quenches.

The appearance of samples after rupture showed a significant difference between heat treatment cycles. The fast ruptures (as-extruded, and water-quenched) showed more extensive and larger blisters than the slower ruptures (slow cooled and annealed). The induction periods for these various heat treatments showed no significant difference. They ranged from 50 to 57 minutes.

Diffusion heat treatment at elevated temperatures produced thick bond layers which are known to be weaker.[18] These samples ruptured at a very high rate. An extreme example is shown which had been heated at 840 C for 60 hours. This sample has a very short (3 minute) induction period, followed by a rapid rupture rate. At the end of the test the cladding was ripped lengthwise and the core was attacked over its entire surface leaving it completely loose within the cladding. Apparently, corrosion progressed rapidly around the entire thick bond causing the cladding to split and separate from the core. The cladding did not blister.

Another sample was heated at 800 C for 16 hours to produce a thick, weak bond. While the attack progressed rapidly around the bond region, it was not as rapid as the sample just previously described. As a result of the rather rapid bond attack, the initial blister spread over a large area before the cladding eventually failed by lengthwise tears. This resulted in a prolonged induction period (75 minutes). The sample then proceeded to rupture rapidly with severe distortion and tearing of the cladding. This kind of behavior appears to be quite similar to the rupture behavior of some fuel elements after reactor irradiation, as will be discussed in a later section.

Zirconium-Uranium Alloy Core

A defect rupture test was performed with a sample of coextruded alloy core rod. The core was a nominal 2 per cent zirconium-uranium alloy clad in 20-mil Zircaloy-2. Hanford analysis of the core material showed a 1.6 per cent zirconium composition. The sample was 0.9 inch in diameter and 2 inches long with a 25-mil defect through the cladding. Prior to exposure the sample was diffusion heat-treated at 850 C for 5-1/2 hours, water quenched, and aged 235 hours at 475 C. It was ruptured in water at 300 C, 1500 psig. The sample and its rupture curve are shown in Figure 35, along with the rupture curve of an unalloyed sample for comparison. It should be kept in mind that the alloy sample was a 0.9-inch diameter rod with 20-mil cladding, and the unalloyed sample was a 0.6-inch diameter rod with 30-mil cladding. These differences would cause some effect, but it would be small compared to the large relative differences in rupture behavior.

The alloy sample had an induction period of 7-1/2 hours compared with 50 minutes for the unalloyed sample. The rupture rate after induction was much slower for the alloy sample; 16 hours to react 50 grams compared with 2 hours to react 50 grams of the unalloyed core. The nature of the rupture was also different for the alloy sample. The initial failure of the cladding for the alloy sample was across the blister at the defect. Additional exposure caused enlargement of the opening by rolling back the edges of the cladding. The cavity in the core after exposure was smooth and rounded. This behavior indicates the absence of hydride penetration down the bond layer or into the core.

Intense irradiation and heat generation in a reactor may decrease the benefits of zirconium additions by damaging the bond layer. Experiments are planned by Coolant Systems Development Operation to investigate these effects.

Slit Defect

A rod element sample was defected with a 30-mil wide slot into the uranium core. The slot was one inch long located centrally on the two-inch sample. In other respects the sample was standard material; coextruded,

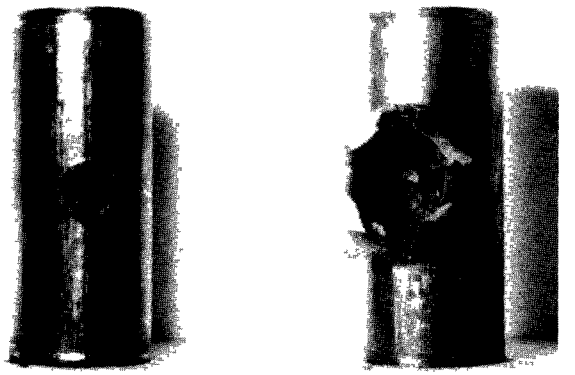

A. After 11-3/4 Hours B. After 25-3/4 Hours

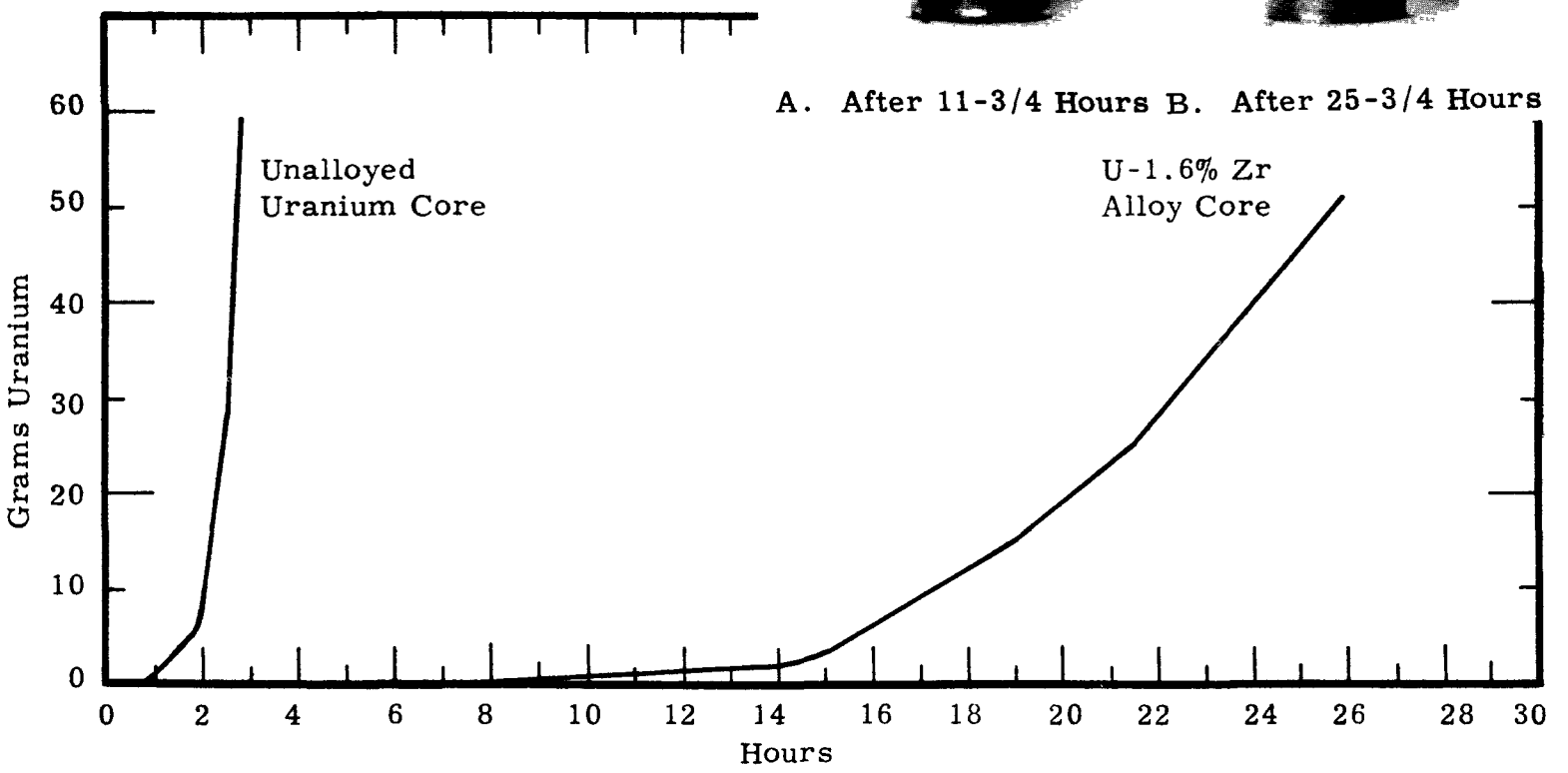

FIGURE 35

Rupture of U - 1.6 Per Cent Zirconium Alloy Core Sample
at 300 C, 1500 psig

30-mil clad, interrupted quench heat treatment. The sample was ruptured in 300 C, 1500 psig water. The sample and its rupture curve are shown in Figure 36. The induction period of 37 minutes was shorter than that observed for a pinhole defect. The rupture curve was essentially the same as for a pinhole defect. This indicated that the geometry of the defect has some effect on the induction period but little or no effect on the rate of rupture.

Tubular Fuel Elements in Water

A series of rupture tests was conducted with tubular coextruded fuel element samples. Samples were 3-inch lengths of 20-mil Zircaloy-2 cladding, uranium core tube with welded, unbonded end closures. They were 1.46-inch ID by 1.85-inch OD with a 25-mil pinhole defect drilled through the center of the outer wall into the core. They were beta treated followed by interrupted quench prior to testing. Two small tube samples were also tested. They were of the same description, but with 0.48-inch ID and 1.06-inch OD.

Rupture curves obtained with the large tube samples are shown in Figure 37. The samples are shown in Figure 38. The induction periods were somewhat shorter than those observed for rod element ruptures. This is probably due, in part, to the thinner cladding employed. Curves A and B are typical rupture behavior at 300 C, 1500 psig. Curve C is greatly accelerated as a result of failure of the inner cladding exposing additional core surface. Curve D is typical rupture behavior at 200 C, 1500 psig. As seen in Figure 38A, the tube ruptures at 300 C are quite similar to rod ruptures inasmuch as they proceed by successive blisters. The possibility of failure of the inner cladding is an additional complication leading to accelerated rates. At 200 C swelling occurs over a large area as a result of extensive hydride penetration of the core (Figure 38B). The remaining uranium in the core had the same spongy appearance typical of attack on rod elements at 200 C.

Effects of Pressure and Core Thickness

The small tube elements were ruptured in 300 C water at 1500 psig and 2500 psig. A sample after rupture is shown in Figure 38C. Their rupture curves are shown in Figure 39. Rupture curves of rod and large tube elements are included for comparison. Increasing pressure increases the rupture rate and decreases the induction period.

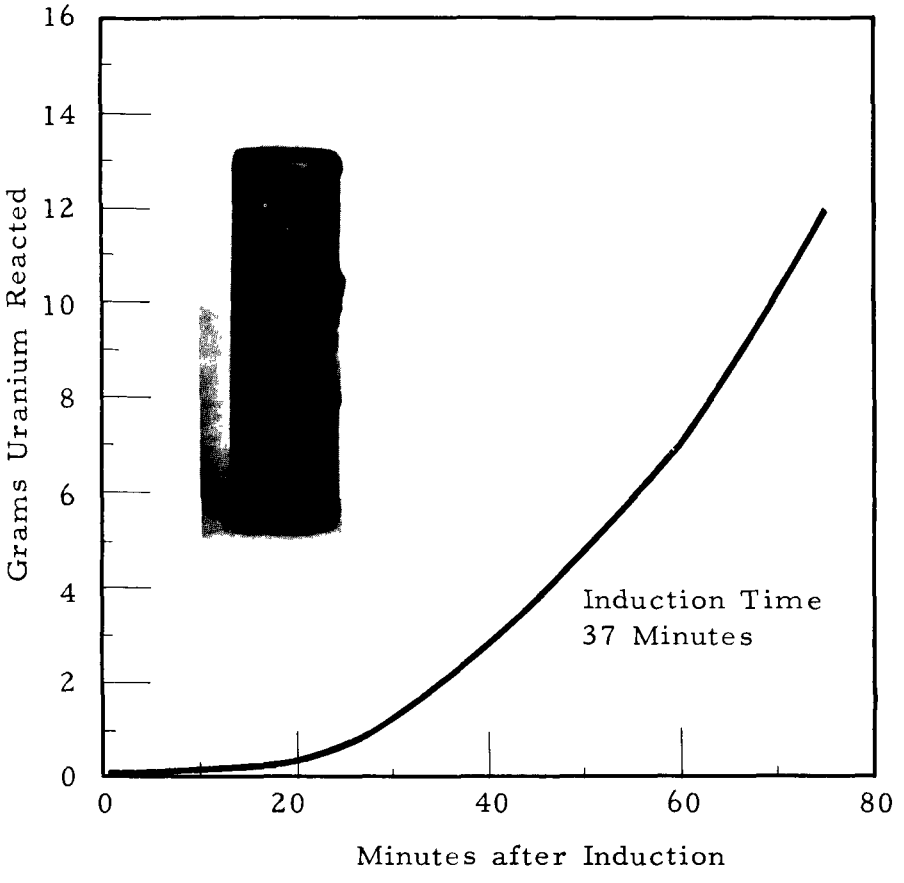

FIGURE 36

Slot Defect Rupture at 300 C, 1500 psig

AEC-GE RICHLAND, WASH

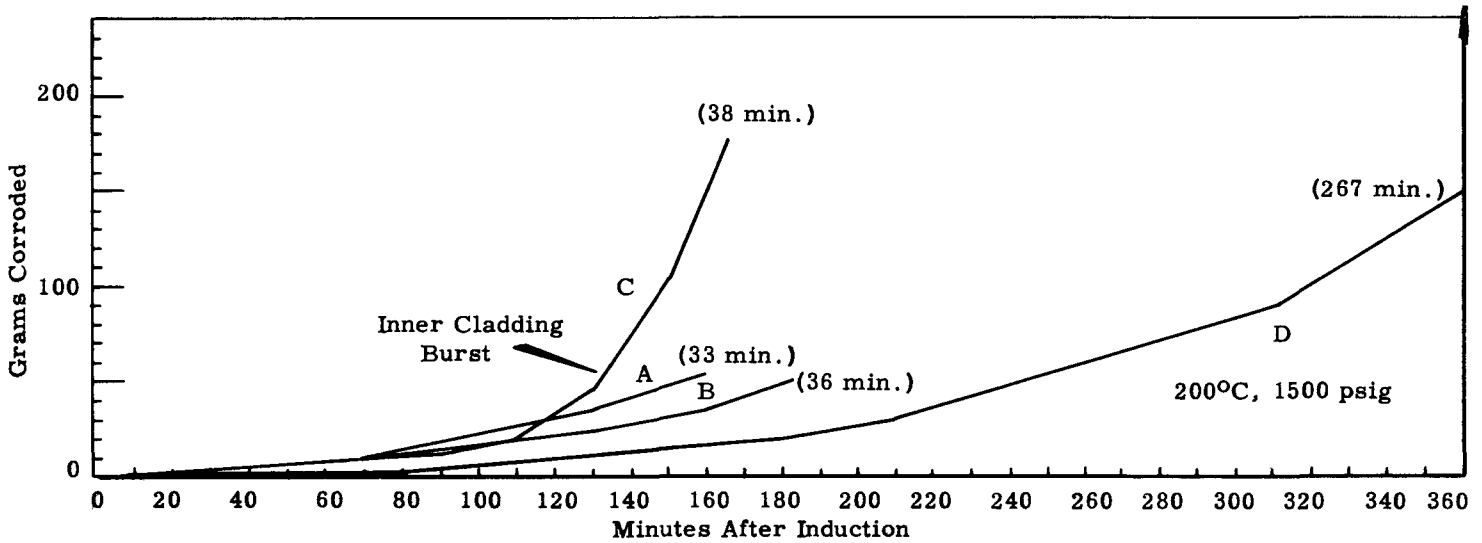

FIGURE 37

Rupture Curves for Large Diameter Tube Elements

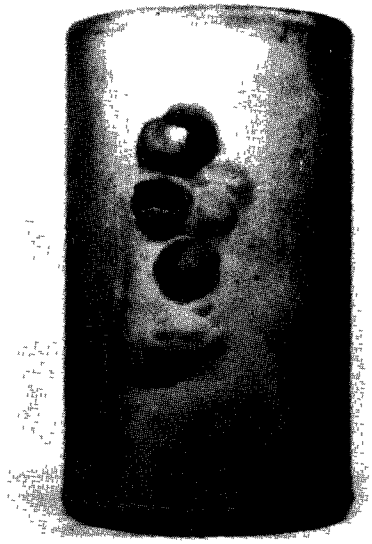

A. Large Diameter Tube Ruptured at 300 C, 1500 psig

B. Large Diameter Tube Ruptured at 200 C, 1500 psig

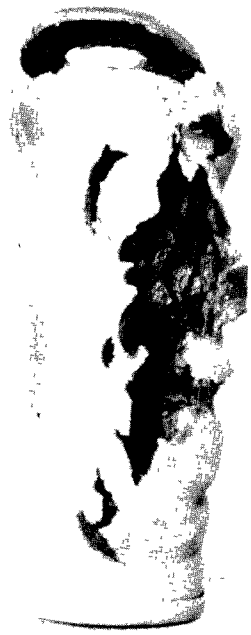

C. Small Diameter Tube Ruptured at 300 C, 1500 psig

FIGURE 38

Ruptured Tube Elements

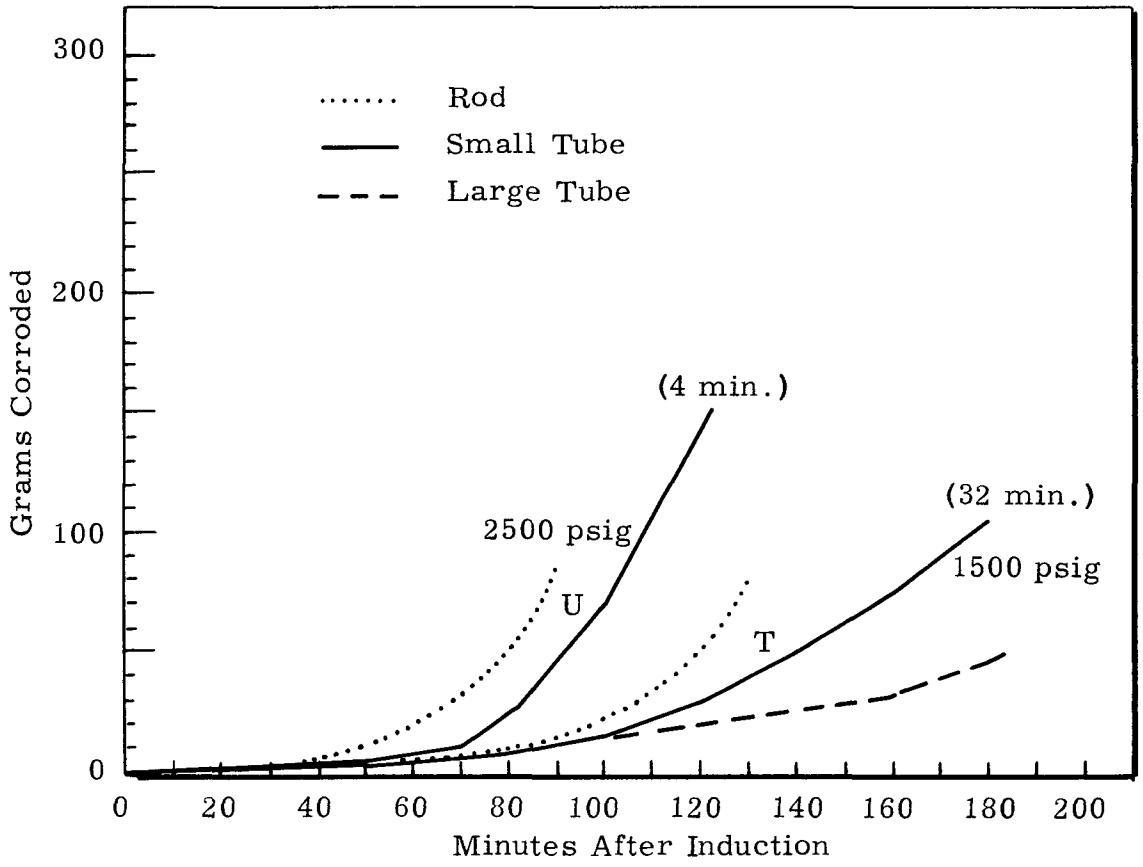

FIGURE 39

Rupture Curves for Small Diameter Tube Elements

AEC GE RICHLAND, WASH

Rupture rates for the small tube elements are more rapid than for large tube elements, and less rapid than rod elements. This is also the order of uranium core thickness for these three types of elements as shown in Table VI.

TABLE VI

EFFECT OF CORE THICKNESS

Element Type	Uranium Thickness	Rupture Rate
Large Tube	0. 14 inch	Increasing rapidity
Small Tube	0. 25 inch	
Rod	0. 53 inch	

The thicker uranium permits greater extension of the corroding surface area resulting in greater acceleration of the rupture rates.

Tube Ruptures with Annular Restrictions

Defected samples of large tube elements were ruptured inside 4. 5-inch lengths of Zircaloy-2 process tubing (2. 09-inch ID, 2. 41-inch OD). Samples were held rigidly in place by means of set screws in the process tubing as shown in Figure 40. The annular space between the defect in the sample and the process tube wall was determined by the position of the set screws. For some tests, the space inside the fuel element was restricted by insertion of a stainless steel plug, or by positioning a stainless steel rod with an extra set of set screws, as shown in Figure 41. All tests were run in 300 C, 1500 psig water.

Sufficient Annulus

Tube element samples, which were not confined in a section of process tubing, behaved in the same manner as rod elements, as previously discussed. When the samples were confined by a process tube, their behavior was dependent on whether the initial blister growing at the defect

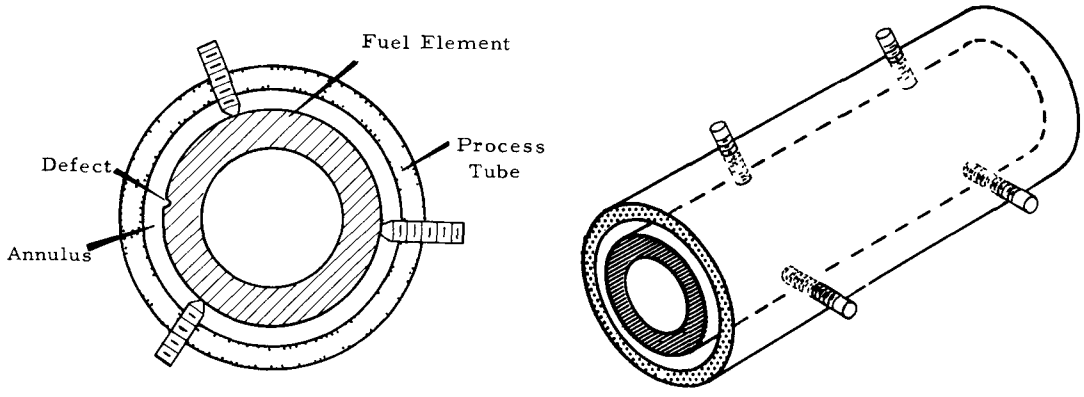

FIGURE 40

Tubular Fuel Element Mounted in Process tube

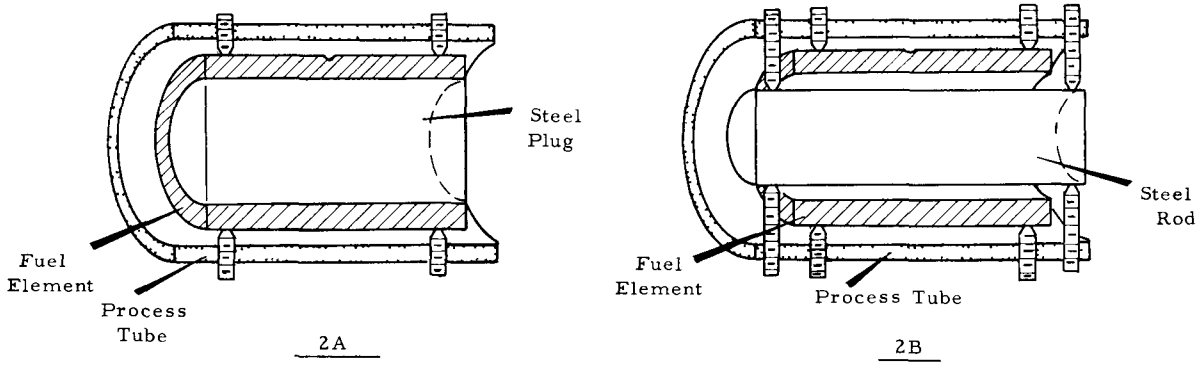

FIGURE 41

Tubular Elements Mounted with Inside Restriction

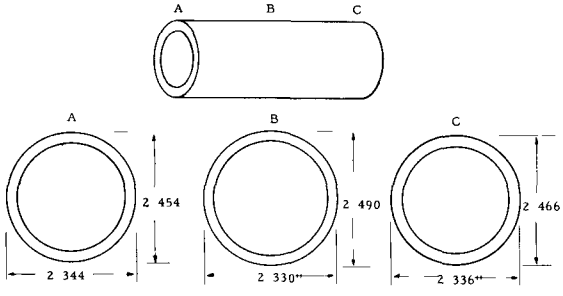

FIGURE 42

Distortion of Process Tubing

was prevented from bursting by restraint of the process tubing wall. When the annulus spacing was sufficient to allow the cladding to burst, the rupture proceeded as though the process tubing were absent as shown in Figure 43. Figure 43A shows a sample in place in a piece of process tubing after the initial blister had burst and released a liter of hydrogen without contacting the process tube. After an additional two hours of exposure the sample appeared as in 43B and 43C. (The set screws are retracted to facilitate photography.) Figure 43C is typical of those large tube samples which ruptured at 300 C without being affected by process tubing. Increasing the annulus spacing increased the probability of this type of rupture behavior.

Restricted Annulus

When there was insufficient annulus spacing to permit unrestricted growth of the initial blister, the process tubing had considerable effect on the rupture. If the blister contacted the wall of the process tube before failure of the cladding occurred, it continued to spread sidewise - mushrooming into the annulus - until the cladding eventually burst. This resulted in a prolonged induction period during which there was little or no release of corrosion products. However, during this time, considerable distortion of the element and process tubing can occur. In one case, for example, the process tube was distorted 0. 16 inch out of round (as shown in Figure 42) before a rupture occurred.

When the cladding finally ruptures, the admission of water to the already damaged core results in a rapid rate of rupture. Figure 44 shows a sample which is typical of those that ruptured under restraint of the process tubing. The sample is shown after the evolution of one liter of hydrogen in Figure 44. Note the mushroomed blister. After an additional two hours of exposure the sample appeared as in Figure 44, B and C. The probability of this type of rupture increases with decreased annulus spacing.

Internal Restriction of Tubular Elements

A stainless steel plug was placed inside one sample as shown in Figure 41A. The sample was centered in the process tubing, giving a 1/8-inch annulus. It was run for two hours after evolution of the first liter of

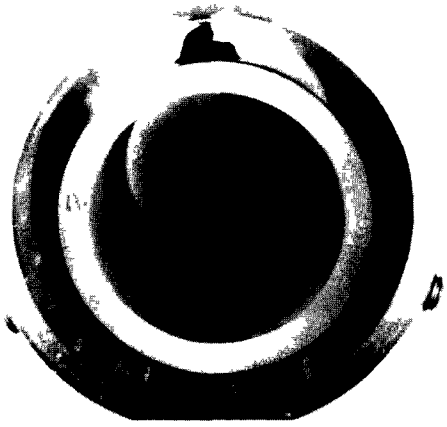

43A. After 1 liter of H_2

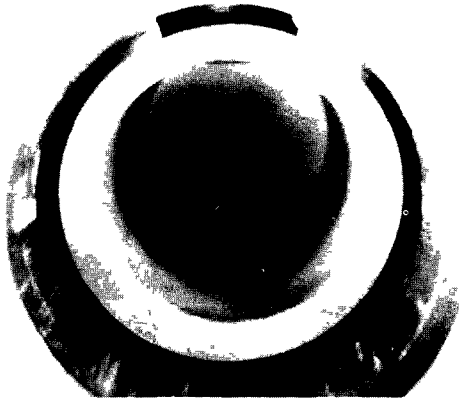

44A. After 1 liter of H_2

43B. Additional 2 Hours

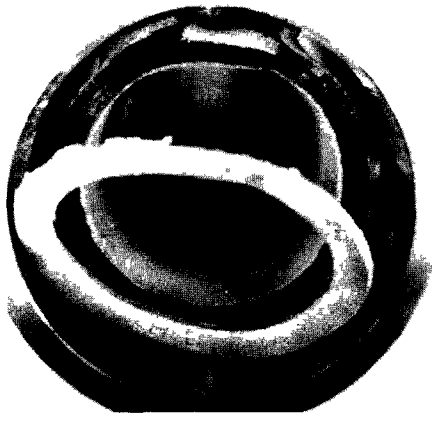

44B. Additional 2 Hours

43C. Process Tube Removed

FIGURE 43

Unrestrained Rupture

44C. Process Tube Removed

FIGURE 44

Restrained Rupture

AEC GE RICHLAND WASH

hydrogen. Because there was no room for inward expansion, all expansion during rupture was directed into the annulus between the element and the process tube. The rupture proceeded rapidly, expanding the sample until it completely filled the annulus, as shown in Figure 45A. (The end cap was detached by the rupture.) After removing the set screws, it was found that the sample was so firmly wedged into the process tube that it could not be driven out with a hammer. It was removed only after the uranium oxide corrosion product was dissolved away (Figure 45B).

Similar tests were run in which an inside annulus of 1/8 inch was obtained by the use of a steel rod, as shown in Figure 41B. One sample is shown two hours after evolution of a liter of hydrogen (Figure 46A), and after removal from the tube (Figure 46B). The rupture was rapid, with the sample expanding and tightly filling both annuli.

1/4-Inch Annulus

Rupture rate curves for samples ruptured in a process tube with 1/4-inch annulus between the defect and the tube wall are shown in Figure 47. Curve E is essentially the same as for an infinite annulus (no process tube). Curve F is somewhat faster as a result of an end cap failure. The rapid acceleration of curve G was caused by the process tube restricting the growth of the initial blister before the cladding burst.

1/8-Inch Annulus

Rupture rate curves for samples ruptured with an 1/8-inch annulus are shown in Figure 48. In curve H, the sample was unaffected by the process tube, and the rupture proceeded essentially the same as for an infinite annulus. Curve J was definitely affected by the process tube, causing a lengthened induction period and a rapidly accelerating rupture.

The sample with its center filled by a steel plug is shown in curve K. With all expansion directed toward the outside, the sample had a short induction time and a rapidly accelerating rate of rupture. The same was true of the samples with an inner annulus fixed at 1/8 inch by a steel rod, as seen in curves L and M.

45A.

45B.

FIGURE 45

Tube Element Rupture with
1/8-inch Annulus
and Center Plugged

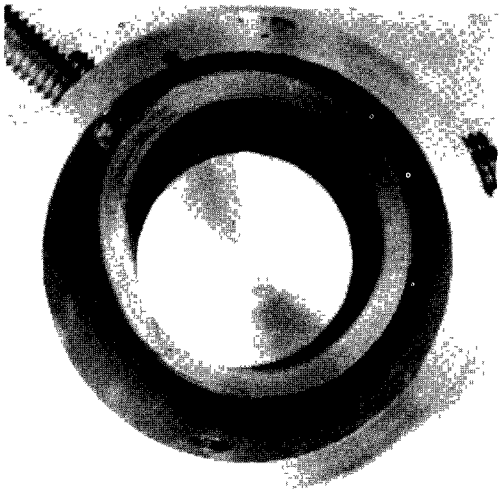

46A.

46B.

FIGURE 46

Tube Element Rupture with
1/8-inch Inner
and Outer Annuli

AEC-GE RICHLAND, WASH.

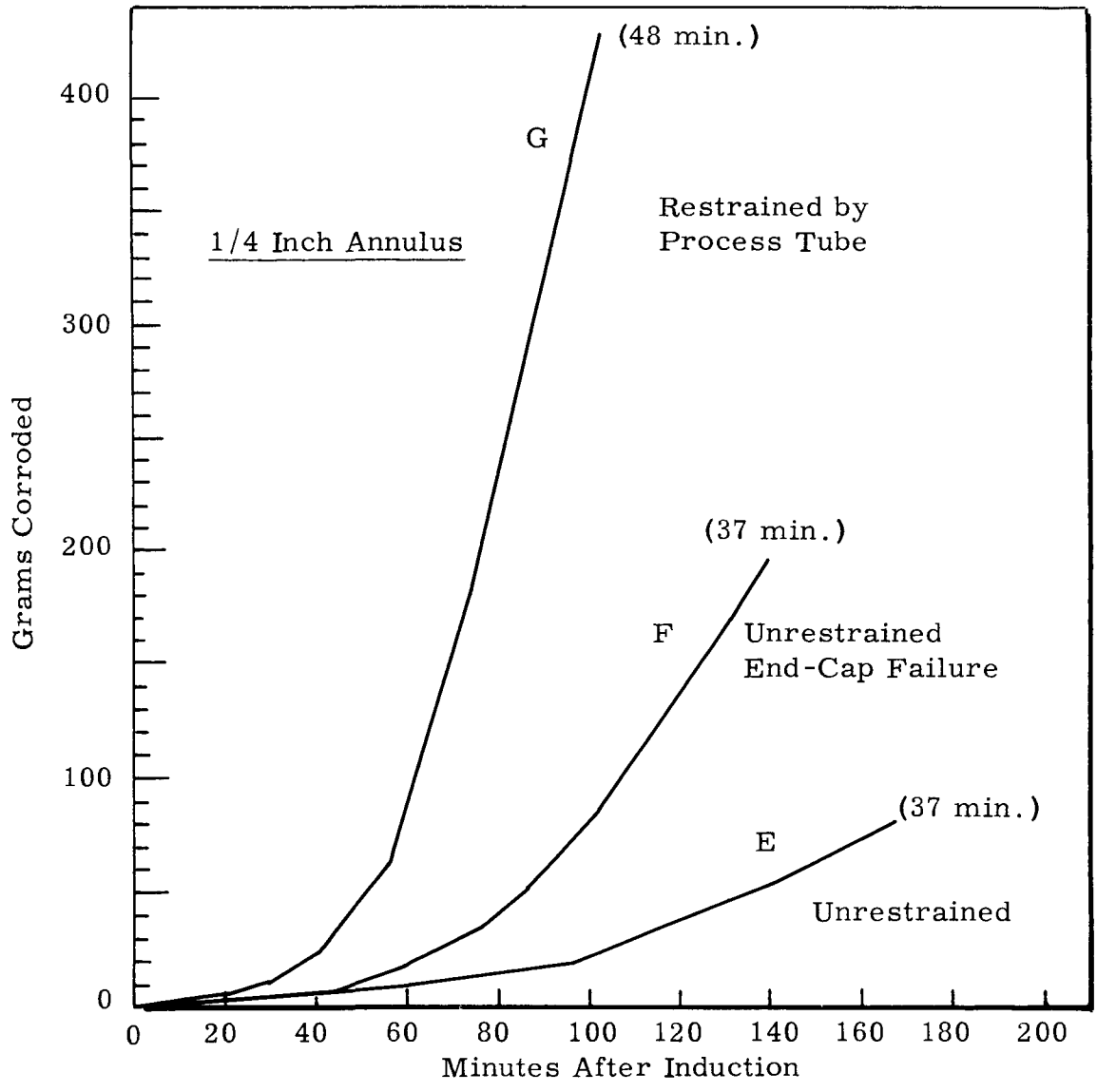

FIGURE 47

Tube Element Ruptures with 1/4-inch Annulus

AEC-GE RICHLAND, WASH.

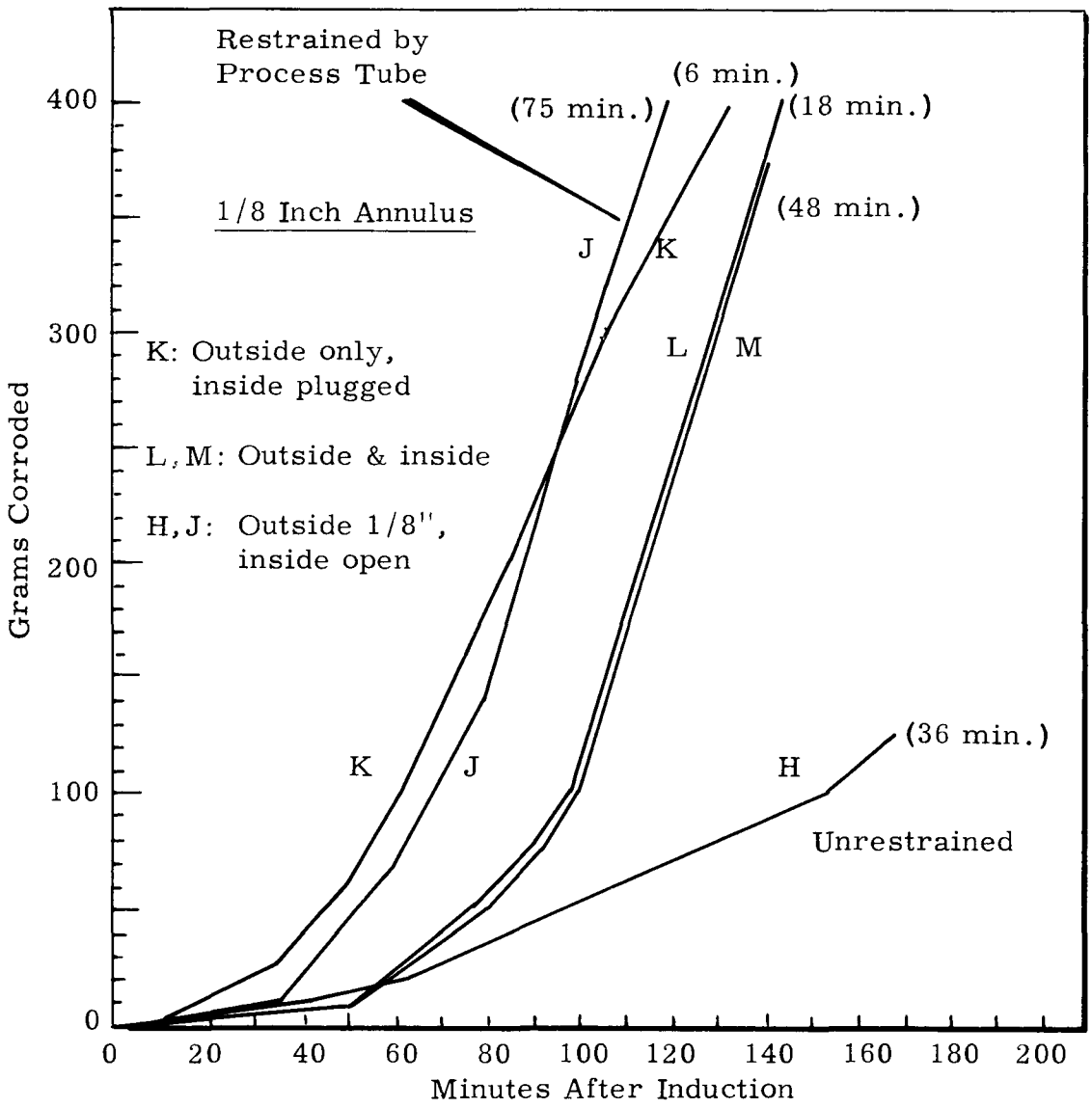

FIGURE 48

Tube Element Ruptures with 1/8-inch Annulus

1/16-Inch and Zero Annuli

Rupture curves for 1/16 inch and zero annuli are shown in Figures 49 and 50, respectively. In all cases there was a prolonged induction period followed by a rapidly acclerating rupture rate.

Summary of Annulus Effects

The results just described for large tubular elements at 300 C and 1500 psig are summarized in Table VII and Figure 51. In Figure 51 all the curves terminating below the dashed line are described as "slow acceleration", as a result of process tube restriction or failure of the end cap or inner wall cladding.

TABLE VII

LARGE TUBE RUPTURES AT 300 C, 1500 psig

Annulus	Induction Period (minutes)	Rate Curve
∞ (no process tube)	33	slow
∞	37	slow
∞	38	rapid
1/4 inch	37	slow
1/4 "	37	rapid
1/4 "	48	rapid
1/8 inch	36	slow
1/8 "	75	rapid
1/8 " (inside plugged)	6	rapid
1/8 inch OD and ID	18	rapid
1/8 inch OD and ID	48	rapid
1/16 inch	100	rapid
1/16 "	420	rapid
0	345	rapid
0	461	rapid

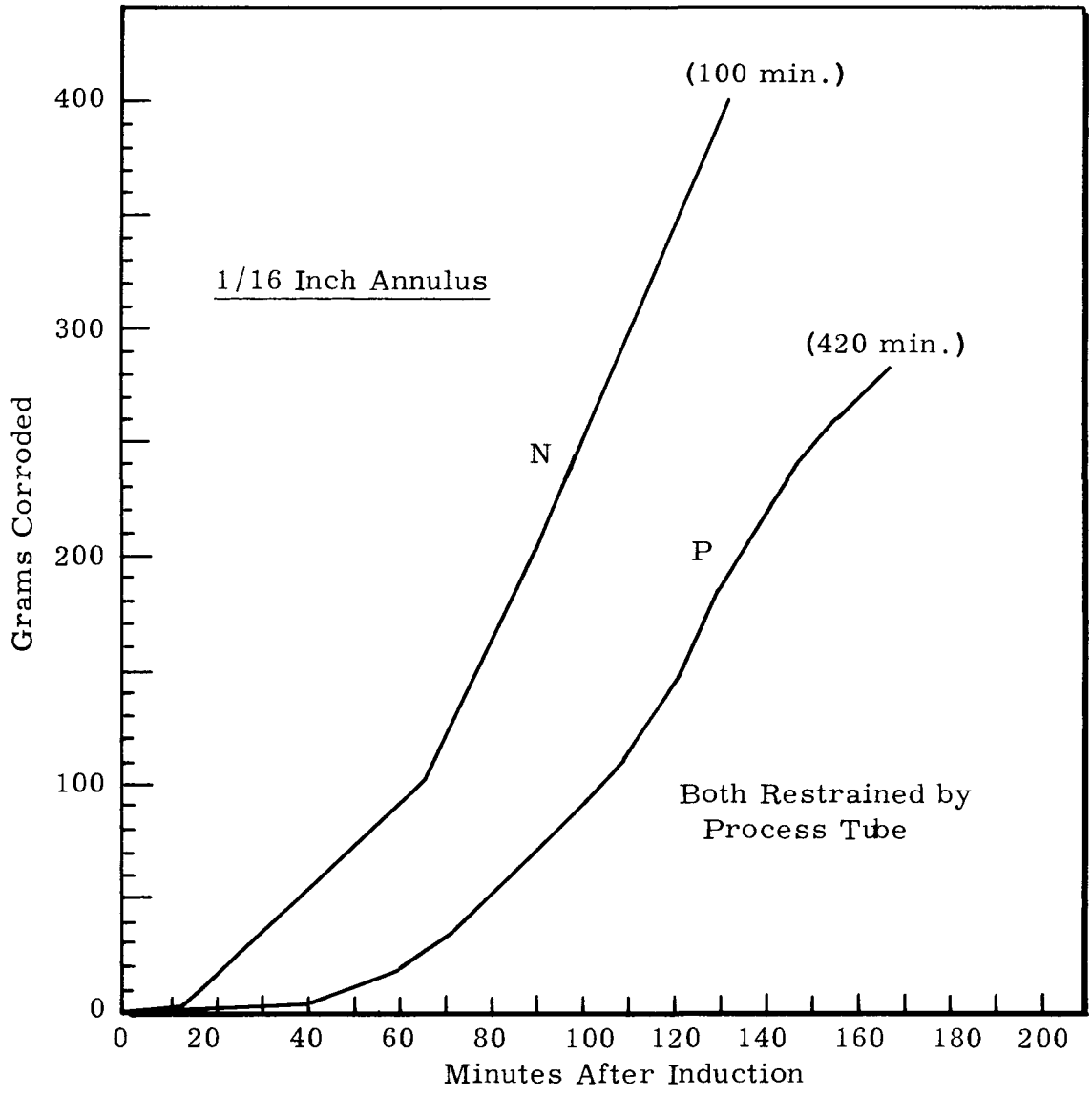

FIGURE 49

Tube Element Ruptures with 1/16-inch Annulus

AEC-GE RICHLAND, WASH

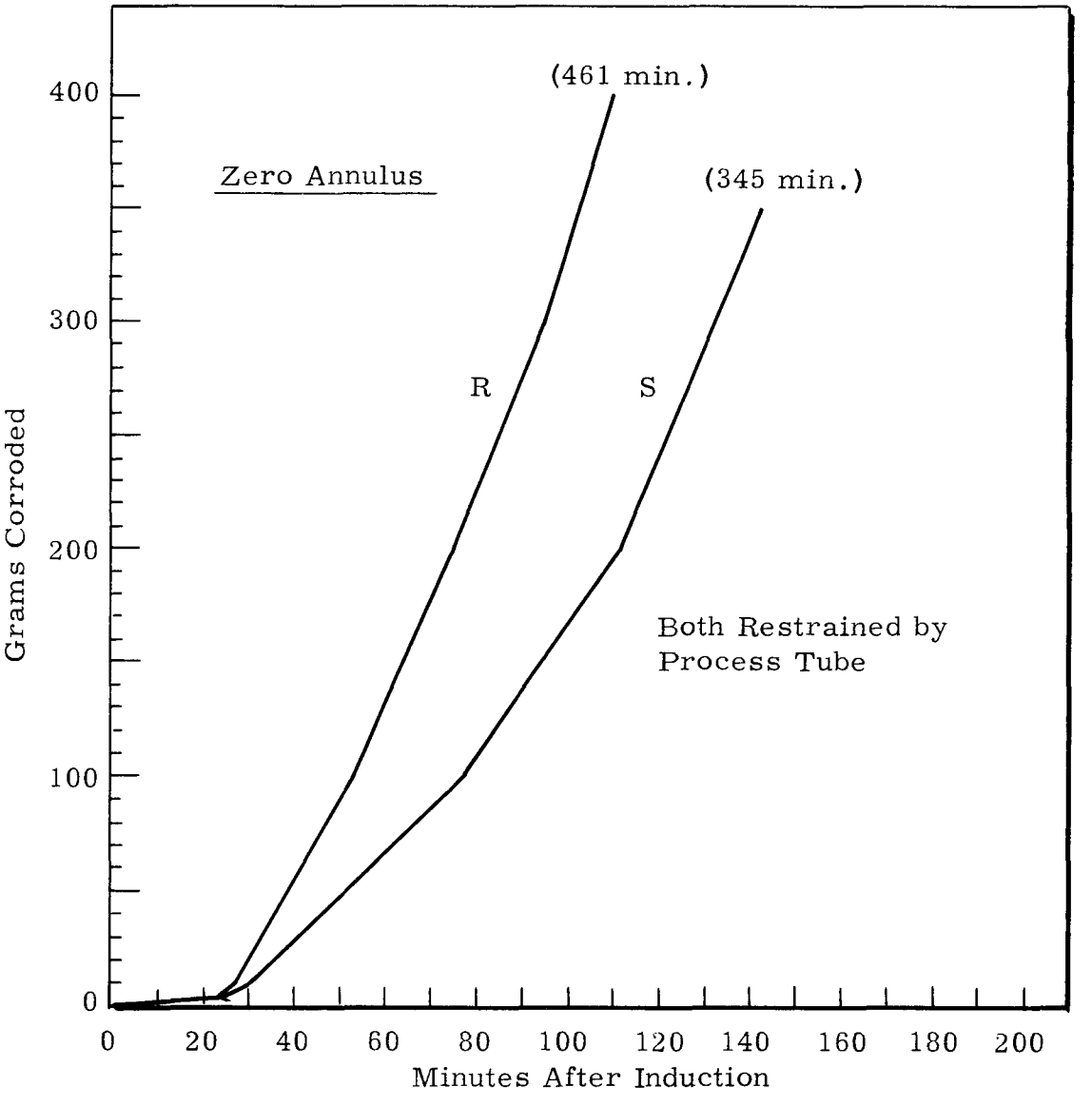

FIGURE 50

Tube Element Ruptures with Zero Annulus

AEC GE RICHLAND, WASH

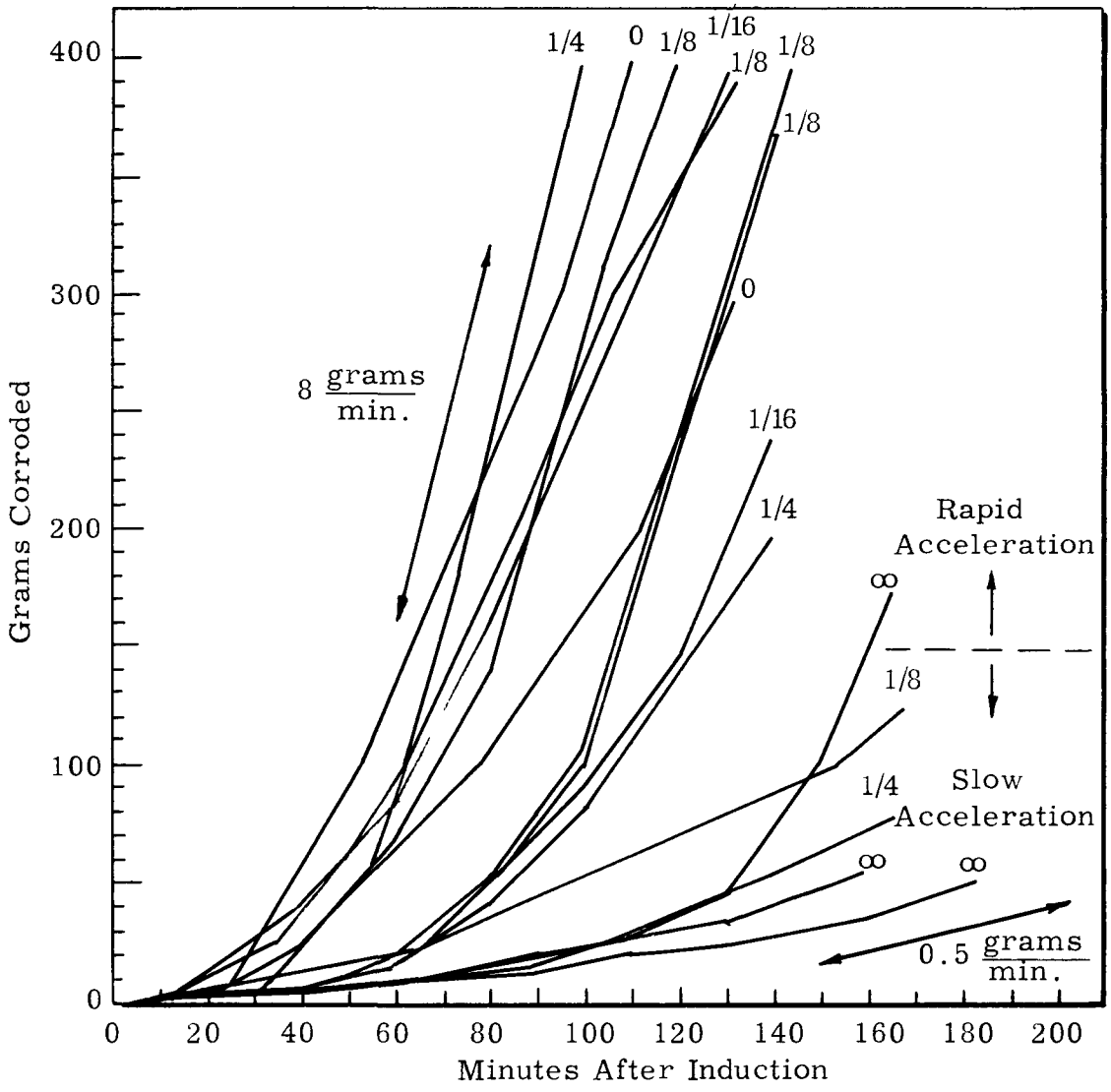

FIGURE 51

Summary of Tube Element Rupture Curves

Normally, the induction period is 30 to 40 minutes followed by a slowly increasing rate of rupture from about 0.1 to 0.5 grams of uranium reacted per minute. If, during the rupture there is an end cap or inner cladding failure, the increase in exposed surface results in a rapid increase in the rate of rupture.

If the outward growth of the initial blister is restricted by the process tube, it mushrooms over the surface of the element and expands inwardly. This prolongs the induction period up to seven or eight hours, during which time considerable distortion of the element and process tube can occur. After the cladding fails, the rupture rapidly increases up to rates as high as eight grams per minute. If inward expansion is restricted, short induction times are observed (5 to 50 minutes) followed by rapidly increasing rupture rates.

In a nuclear reactor, cooling water is circulated in the annuli between the fuel elements and process tube. If the initial blister on a defective element mushrooms into the annulus, it appears possible that a significant flow blockage could occur before the blister bursts and the rupture is detected. For instance, the sample in Figure 44A had obstructed about 15 per cent of the annulus before the cladding burst. Two hours later the annulus was about 95 per cent blocked (Figure 44B). A blister of the type formed at 200 C (Figure 38B) would certainly cause extensive flow blockage. Inner and outer annuli of 1/8 inch were from 95 to 100 per cent blocked two hours after induction (Figure 46A).

Inner Cladding Defect

Only one test was conducted in which the inner cladding of a tubular element contained the pinhole defect. The sample was a small tube element with a 25-mil pinhole defect, exposed at 300 C, 1500 psig. This test was run to provide a comparison for an in-reactor rupture; and, consequently, it was not allowed to progress very far. A section of the sample after rupture is shown in Figure 61. The induction period was 63 minutes , which is about twice as long as for a small tube with an outside cladding defect (32 minutes - see Figure 39). After cladding failure, the element ruptured at a rate of

about 2.7 grams per minute, which is considerably higher than the outside cladding case. The rupture test was terminated six minutes after induction, so the later stages of rupture were not studied.

It appears that the additional strength of the inner cladding, because if its "inverted" geometry, resists failure, resulting in a prolonged induction period during which there is more extensive internal reaction. Failure of the cladding then results in a rapid rate of attack.

Fuel Element Ruptures in Steam

The preceding sections have dealt with various aspects of the rupture behavior of fuel elements in water. In the case of a power-generating fuel element, the temperature of the core material is considerably higher than the coolant water. In this case, if water penetrates a defective cladding, it would be converted to steam and the rupture would proceed by a uranium-steam reaction at a temperature above that of the bulk coolant. Even with the reactor shut down, the gamma heating of the irradiated uranium might be sufficient to convert the water to steam. The uranium-steam reaction would continue until the opening in the cladding was large enough to admit sufficient water to cool the exposed core surface below the boiling point of the water. Clearly, then, the rupture behavior of fuel elements in steam is pertinent to the rupture behavior of a fuel element in a reactor. In addition, the steam reaction is important with respect to fuel failures which occur during autoclave "proof-testing". This proof-testing of Zircaloy clad fuel elements prior to reactor exposure is usually done in 400 C steam.

Rod Element Ruptures in Steam

Pinhole-defected rod elements (coextruded, 0.6-inch OD, 2 inches long) were ruptured in steam at temperatures from 225 to 500 C and pressures from 200 to 2000 psig. The ruptured samples are shown in Figure 52. The conditions of exposure and the induction periods are listed in Table VIII. Rupture rate curves, based on hydrogen collection, are shown in Figure 53.

A. 500 C
2000 pisg

B. 500 C
1000 psig

C. 500 C
200 psig

D. 450 C
1000 psig

E. 450 C
200 psig

F. 400 C
2000 psig

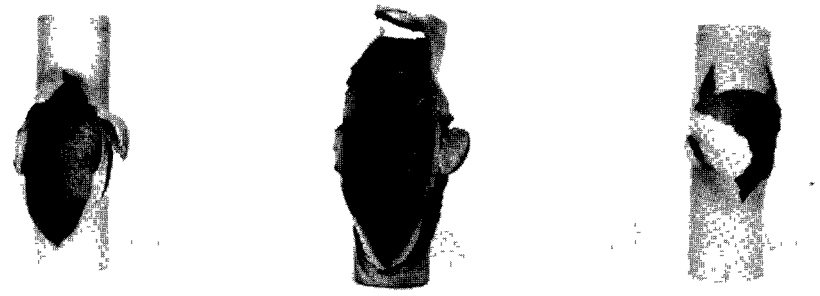

G. 300 C
1000 psig

H. 300 C
200 psig

J. 225 C
200 psig

FIGURE 52

Rod Elements Ruptured in Steam

AEC-GE RICHLAND, WASH.

TABLE VIII

ROD RUPTURES IN STEAM

(25 mil defect)

Sample	Temperature	Pressure	Induction Period
A	500 C	2000 psig	16 minutes
B	500	1000	20
C	500	200	63
D	450	1000	21
E	450	200	45
F	400	2000	25
G	300	1000	57
H	300	200	153
J	225	200	672

The induction time prior to rupture is similar to that in water. For comparison, the induction time in water at 300 C, 1500 psig is 50 to 70 minutes. Induction times decrease with increasing temperature and pressure. During the induction time, a blister forms in the cladding at the defect site similar to the observed rupture behavior in water. The induction period is terminated by failure of the cladding at the base of the blister giving the first release of hydrogen and uranium oxide corrosion products. Rupture then proceeds in a manner quite different from that in water. Because of the poor heat transfer properties of steam and the insulation offered by the oxide corrosion product, the heat generated by the corrosion of the uranium core greatly increases the temperature of the uranium. This leads to rupture rates much higher than those experienced in water. For comparison, a water rupture curve is shown in Figure 53. In water, a rupture proceeds by successive blister formation; whereas in steam the major attack is into the core, resulting in a large opening accompanied by lengthwise tearing and brittle failure of the cladding.

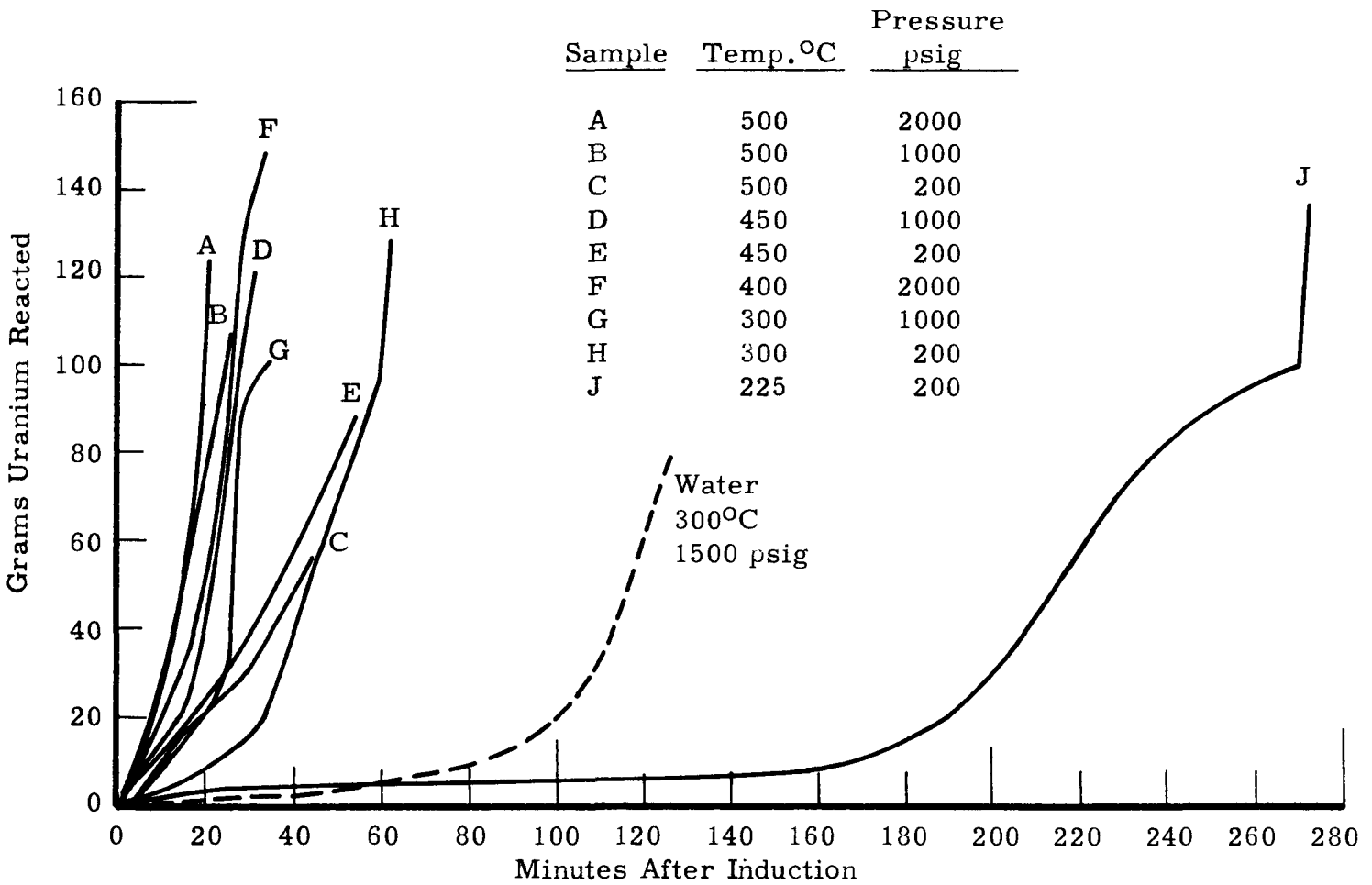

FIGURE 53

Rupture Curves for Rod Elements in Steam

Rupture rates are essentially the same at 400 C, 450 C, and 500 C at 1000 and 2000 psig. At 200 psig the rates are somewhat lower. At 225 C, 200 psig, the initial rate of rupture is quite low. At 300 C, 1000 psig (sample G) a very high rupture rate of about 50 grams per minute occurred during the run. This occurred apparently as a result of a brief downward excursion of the temperature, during which the steam condensed. The same behavior was observed at the termination of tests H and J. A brief high rate of reaction was observed when the steam condensed to water as a result of cooling the autoclave. The reason for the acceleration in rate is not known at this time, but it is possibly due to the reaction of uranium hydride with water liberating hydrogen.

Many of the foregoing conclusions were confirmed by a rupture experiment conducted in the direct viewing unit. A fuel element sample was observed visually as it ruptured in 310 C, 1000 psig steam. After formation of the initial blister at the defect site, the cladding opened lengthwise and appeared as in Figure 52B. Occasionally, portions of the uranium oxide fell out of this cavity exposing the bare uranium for a brief period. The uranium was glowing at an orange-red heat and the temperature was estimated at about 700 C. The steam temperature measured adjacent to the sample maintained a constant 310 C. Just before the test was terminated, the temperature was lowered to 285 C, causing the steam to condense to water. When the water encountered the uranium, the rupture rate increased for about a minute and then slowed down as the whole assembly was cooled.

Tube Element Ruptures in Steam - Effect of Steam Pressure and Defect Size

Seven tubular fuel element samples were rupture-tested in 400 C steam. The purpose of this series of tests was to determine the effect of defect size and steam pressure on rupture behavior. More specifically, these tests were run to evaluate the autoclave proof-testing procedure by determining the defect detecting capabilities of 400 C steam at various pressures.[24] The samples were two-inch lengths of coextruded Zircaloy-2 clad, uranium core tube with welded, unbonded end closures. They were 2.47-inch OD, 1.85-inch ID, with 20-mil thick inside and outside cladding. The test conditions and observed induction periods are given in Table IX. Rupture curves are given in Figure 54.

TABLE IX

TUBE ELEMENT RUPTURES IN 400 C STEAM

Sample	Pressure (psig)	Defect Diameter (mils)	Induction Time
T-1	1500	25	27 minutes
T-2	100 and 1500	25	Ran 17 hours at 100 psig with no reaction. Failed 10 minutes after increasing pressure to 1500 psig.
T-3	1500	10	27 minutes
T-4	1000	10	42 minutes
T-5	500	10	No rupture after 6-3/4 hours
T-6	100	10	38 hours
T-7	1500	3	21 minutes

Comparison of the data obtained at 1500 psig shows no effect of defect diameter on the induction time over the range of 3 to 25 mils. Decreasing the pressure below 1000 psig greatly prolongs the induction time. Sample T-6 is shown at various stages of exposure in Figure 55. Even after 26 hours, there was only a slight blister visible. Since the induction time was 38 hours, the blister must have grown rapidly prior to failure.

The curves of Figure 54 show little difference in the rupture rates of all the samples with the exception of T-6 (10-mil defect, 100 psig) which ruptured at a slower rate. Comparison of these curves with those in Figure 53 shows the tubular elements rupture slower than the rod elements under similar conditions. This observation is consistent with that previously discussed for water behavior. The greater thickness of uranium in the rod elements permits greater acceleration of the rupture rates.

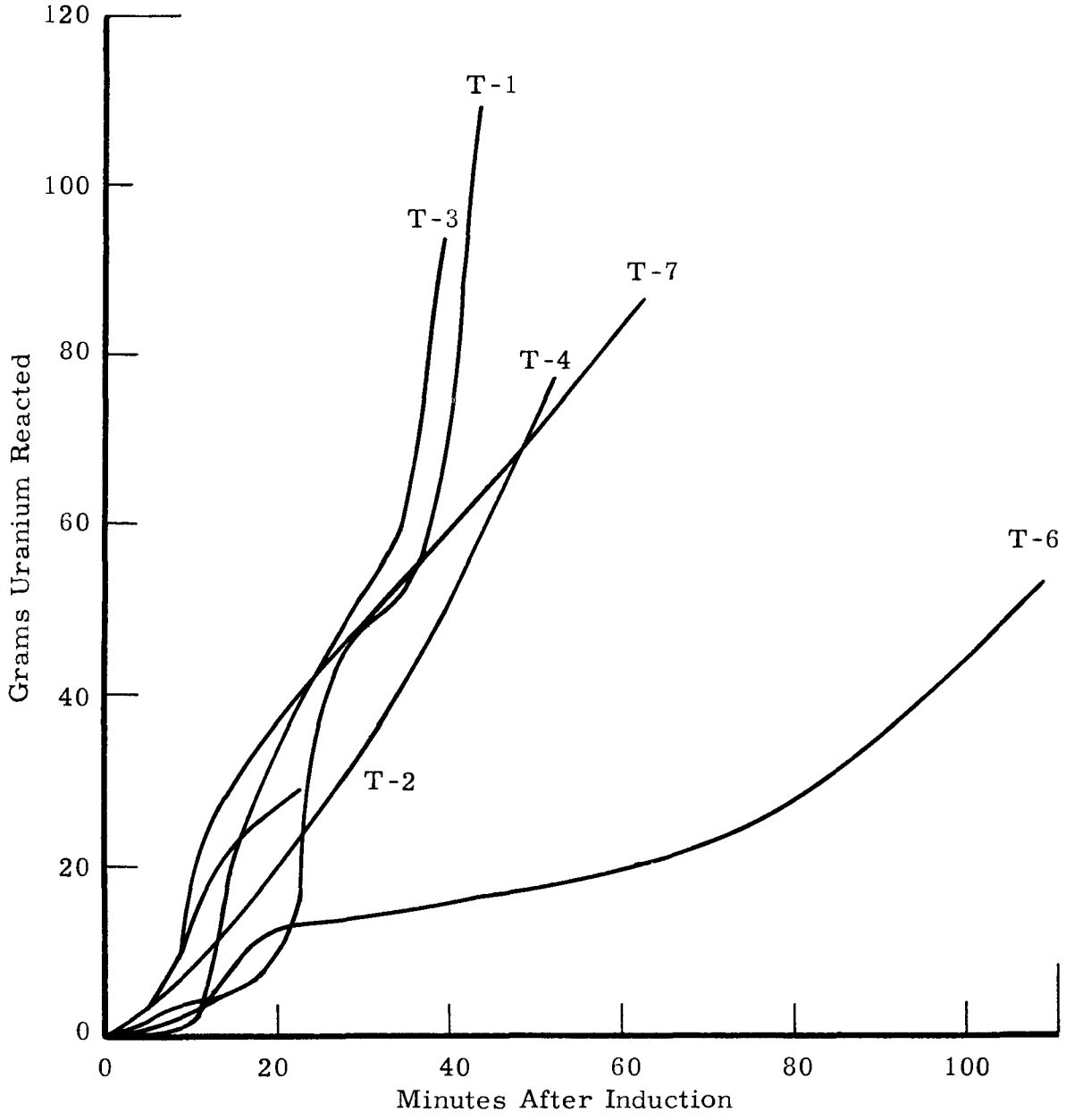

FIGURE 54

Rupture Curves for Tube Elements in Steam

AEC-GE RICHLAND, WASH

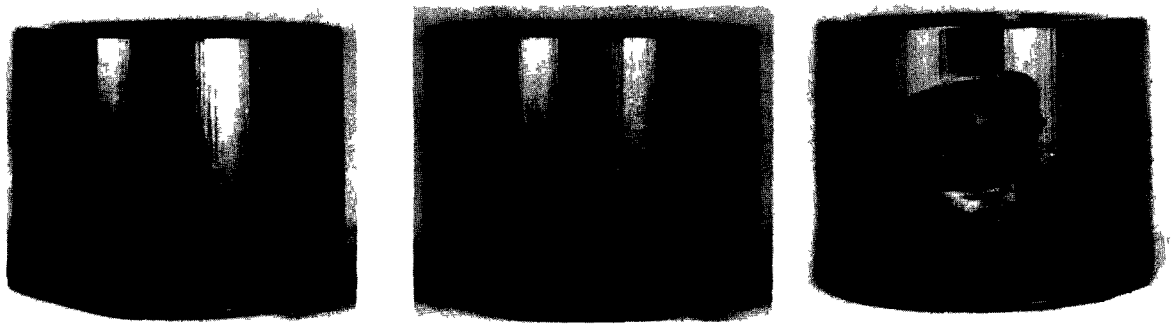

24 Hours

36 Hours

40 Hours

FIGURE 55

Rupture of Tubular Element with 10 mil
Pinhole Defect in Steam at 400 C, 100 psig

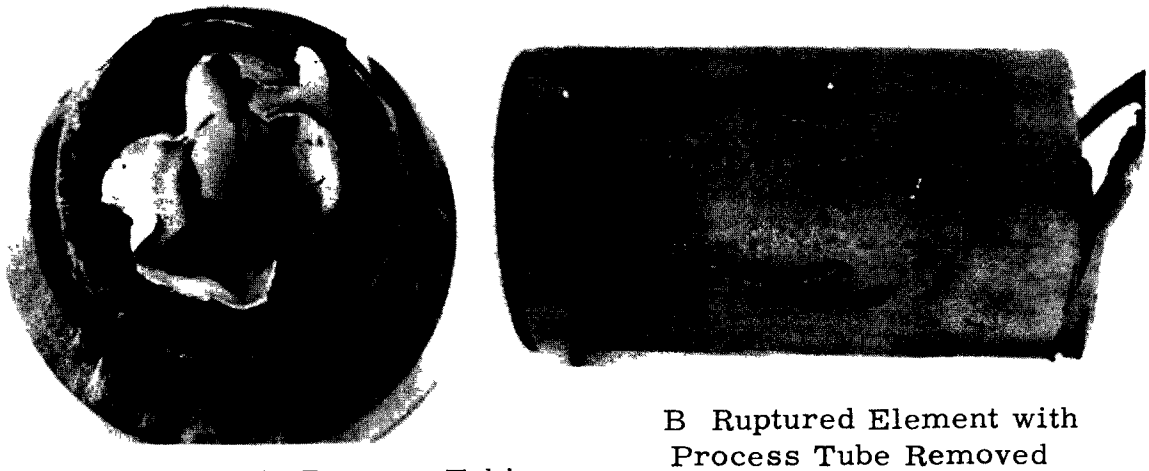

A In Place in Process Tubing

B Ruptured Element with
Process Tube Removed

FIGURE 56

Tube Element Ruptured in Process Tubing

AEC GE RICHLAND WASH

Hydriding of Zircaloy Components

A question of considerable importance is the extent of hydrogen picked up by Zircaloy components in the neighborhood of a fuel element rupture. A rupturing fuel element generates about one liter (STP) of hydrogen for each five to seven grams of uranium reacted. Zirconium has a strong tendency to pick up hydrogen and become embrittled. The presence of water is known to reduce or eliminate the pickup of molecular hydrogen by Zircaloy.

Whether a Zircaloy process tube has acquired damaging amounts of hydrogen from a fuel element rupture is very important. Replacement of the process tube after a rupture is costly and unnecessary if there has been no damaging hydrogen pickup. On the other hand, if the process tube has hydrided significantly, then continued operation creates a serious hazard to the reactor.

Whether the Zircaloy cladding of fuel elements adjacent to a rupture picks up damaging amounts of hydrogen is of relatively little importance since these elements would be discharged along with the ruptured element. The extent of hydriding of the cladding on fuel elements adjacent to a fuel failure during autoclave "proof-testing" is quite important, however, since this will determine whether these elements can be used or whether they must be discarded.

Figure 56 shows a tubular fuel element which was ruptured in 300 C, 1500 psig water. The sample was placed in a length of Zircaloy-2 process tubing with the sample defect wedged against the inside wall of the process tubing. During the rupture of this element about 550 grams of uranium were reacted liberating 78 liters of hydrogen. The process tube was sectioned and examined metallographically. There was no pickup of hydrogen by the process tube.

A series of tests was conducted in which Zircaloy-2 samples were positioned near a rupturing fuel element sample. Tests were conducted in steam at 500 C and 400 C, 2000 psig; and 310 C, 1000 psig. The fuel samples were pinhole-defected rod elements. The Zircaloy samples were strips of

sheet 1/4 inch wide, 6 inches long, and 30 mils thick. Two samples were used in each test; one in the as-etched condition, and one with an autoclave-produced corrosion product film (formed in 400 C, 1500 psig steam for 72 hours). They were rigidly mounted 1/4 inch away from the defected element and were spread 1/8 inch apart. The sample arrangement is shown in Figure 57. The samples are shown after exposure in Figure 58. The Zircaloy strips were cut in thirds and analyzed for hydrogen content by vacuum extraction. Samples of Zircaloy were exposed to 500 C, 2000 psig steam without a fuel element to determine the hydrogen pickup associated with the steam corrosion. Control samples were analyzed to determine hydrogen content in the as-etched and as-autoclaved conditions.

The three analyses for each sample were in close agreement and showed no significant variation from top to bottom of the strips. The results are given in Table X.

TABLE X

HYDROGEN PICKUP BY ZIRCALOY ADJACENT TO A RUPTURE IN STEAM

Temperature (C)	Pressure (psig)	Total Exposure (min)	Period of Hydrogen Evolution (min)	Hydrogen Evolved (liters)	Hydrogen Analyses	
					Etched (ppm)	Autoclaved (ppm)
Control	--	--	--	--	21	42
500 no rupture	2000	168	--	--	60	30
500	2000	168	24	8.8	82	35
400	2000	145	63	10	28	29
310	1000	166	70	11	27	36

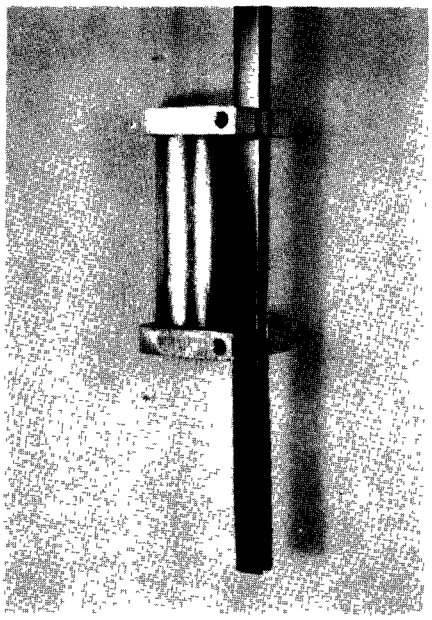

FIGURE 57

Sample Arrangement

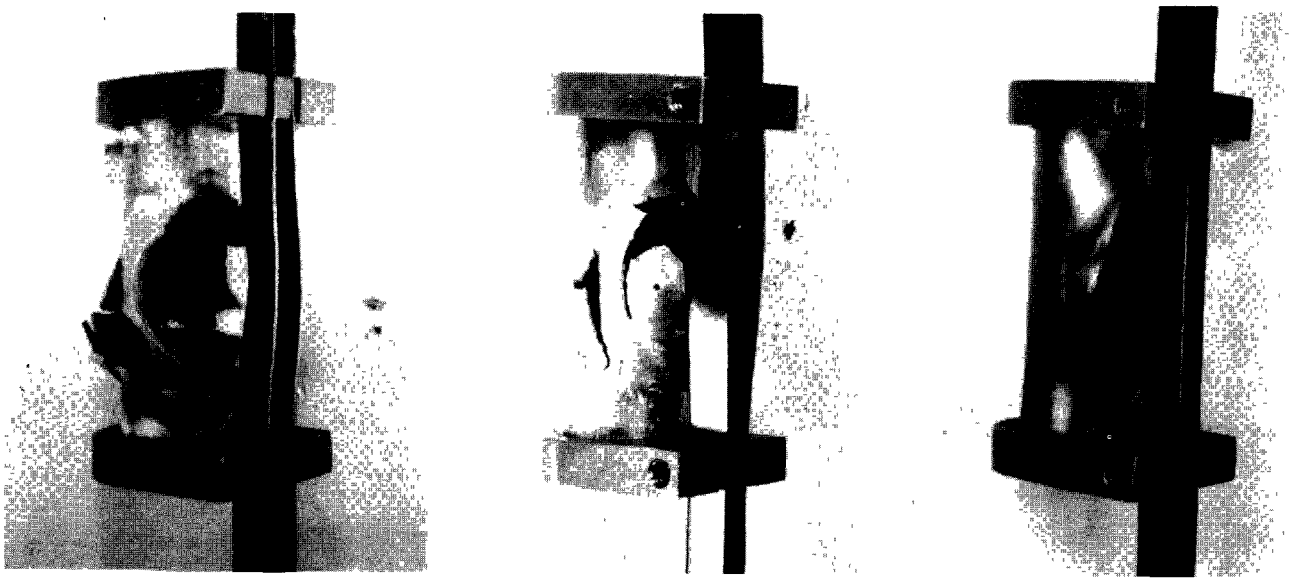

A. 500 C
2000 psig steam

B. 400 C
2000 psig steam

C. 310 C
1000 psig steam

FIGURE 58

Steam Ruptures with Adjacent Zircaloy

Examination of the hydrogen analyses of the autoclaved Zircaloy specimens shows no increase in hydrogen content as a result of exposure with or without a fuel rupture. The values, ranging from 29 to 42 ppm, indicate the variation in hydrogen content after pretreatment autoclaving. This represents an increase of 8 to 21 ppm over the as-etched condition. The samples used in the as-etched condition showed small increases in hydrogen content at 310 C and 400 C, but these are attributable to corrosion of the Zircaloy rather than pickup from the adjacent rupture. At 500 C the hydrogen content of the as-etched sample increased 39 ppm in the absence of a rupture, and 61 ppm in the presence of a rupture. The difference, 22 ppm, is attributable to hydrogen pickup from the rupture during the 24 minutes that it was evolving hydrogen.

It can be concluded that even with steam temperatures as high as 500 C, for short exposures Zircaloy located close to a hydrogen-generating fuel rupture will not pick up hydrogen, provided it has an intact corrosion product film. If the corrosion product film is damaged (as simulated by the as-etched specimens), no hydrogen is picked up from a nearby rupture at 400 C or less, and only a small amount is picked up at 500 C. The pickup at 500 C is even less significant when the mass/area ratio of the Zircaloy is considered. The test samples had a ratio of 0.24 grams per square centimeter, whereas a process tube would have a ratio of about 4.5 grams per square centimeter of inside wall area. This means that the amount of hydrogen which gives an increase of 22 ppm in the test samples, would give an increase of only 1.2 ppm in an equivalent area of process tubing.

All of the elements ruptured in steam at 400 C and above showed signs of brittle cladding failure indicating extensive hydriding of the cladding. These elements are shown in Figures 52 and 58. At 300 C there is some indication of hydriding of the cladding. It has been shown that Zircaloy adjacent to a rupture in steam does not hydride up to 500 C. It follows, there, that the extensive hydriding of the cladding must occur from within, as previously shown in Figure 14 and discussed in the earlier section on "Nature of the Nonuniform Attack."

There are two important practical results of the Zircaloy hydriding studies. In the event of a fuel element rupture in a Zircaloy reactor process tube, no hydrogen damage to the tube should occur, provided the coolant has not been completely blocked (creating a dry atmosphere) and the tube temperature has not exceeded 500 C. Above 500 C data are not available. In the event of a dry atmosphere caused by severe coolant flow blockage, hydrogen damage to the process tube would surely result. In the event of a fuel element failure during autoclave "proof-testing" in 400 C steam, no hydrogen damage to adjacent elements should occur, provided the rupture is not permitted to become so rapid and extensive that elevated temperature and dry hydrogen conditions are attained. In both the cases of a rupture during autoclave or reactor exposure, rapid detection and cool down during the early stages of rupture will eliminate the possibility of hydrogen damage to adjacent Zircaloy components.

Comparison of Autoclave and Loop Rupture Behavior

Effects of Coolant Flow

All the tests previously described were conducted in static or slowly refreshed autoclave systems. In order to evaluate the effects of coolant flow past a rupturing element, a series of rupture experiments were conducted by K. D. Hayden, Coolant Systems Development Operation, and J. W. Goffard, Fuel Element Design Operation, in an out-of-reactor loop.[19] They found that coolant flow of eight feet per second had little or no effect on the induction period or the subsequent rate of rupture. They did find, however, that coolant flow reduced the extent of cladding blistering in some cases. Samples, which had been beta heat treated and quenched in a manner to give the slowest rupture rate (isothermal quench, for instance), formed only the initial blister at the defect. Subsequent corrosion removed uranium without the formation of additional blisters. Those samples which were heat treated to give the faster rupture rates (for example, water quenched), failed in a manner similar to autoclave behavior with successive blistering of the cladding. This effect of coolant flow can be understood by reference to the mechanism illustrated

in Figure 29. In addition to the direct oxidation of the uranium core, a rupture progresses by hydrogen penetration down the bond layer giving a uranium hydride front which undercuts and blisters the cladding.

If the bond layer is easily penetrated by hydrogen, then the hydride can form at a site sufficiently removed from the rupture cavity that cooling water does not affect it. This would be the case, for example, with a water-quenched element, where blistering proceeds in spite of the flow of cooling water into the rupture cavity.

If the bond layer is not easily penetrated by hydrogen, then water flow into the rupture cavity will sweep out the uranium oxide and inhibit the formation of uranium hydride. This is presumably the case for the isothermal-quenched element which blisters in a static system (where oxide in the cavity protects the hydride from the water), and does not blister in a flowing system (where water flow sweeps out the oxide and inhibits hydride formation).

At 200 C where hydrogen penetrates rapidly and deeply into the uranium and away from the original reaction site (Figure 30), it is probable that coolant flow will not affect the rupture behavior. This case has not as yet been experimentally investigated.

As previously discussed in the section on ruptures in steam, limited access of water through a small defect into a power-generating core, which is substantially hotter than the ambient water, can lead to a uranium-steam reaction and burning of the core. Coolant flow into the rupture site will remove the insulating oxide and carry away the heat, thus cooling the rupture until it is essentially proceeding in water at ambient temperature. The rapidity with which the water can cool the rupture is dependent upon the ease with which water can enter the rupture site. This in turn is dependent on the geometry of the rupture and the flow rate of the water.

Effects of Heat Generation

As previously discussed, water entry through a small cladding defect into a heat generating uranium core could conceivably result in a uranium-steam reaction. K. D. Hayden has performed an experiment in a recirculating loop where the defected fuel element sample was resistance heated[20]

to simulate the rupture of a power-generating element. The sample was an as-extruded 0.6-inch diameter rod with 30 mil cladding and 25 mil pinhole defects. It was run at 300 C, 1650 psig, 20 feet per second water flow, and 30 kilowatts per foot electrical power generation.

No significant effects of heat generation were observed. Coolant flow was high enough to sweep the oxide out of the rupture site. This high rate of coolant access to the core apparently prevented a uranium-steam reaction. This is probably what will happen in the case of an in-reactor rupture; once the cladding has actually failed, sufficient coolant water will enter to prevent a steam reaction and the rupture will proceed in water at, or near, ambient temperature. In the event of a coolant blockage, however, a "steam rupture" of a power-generating element is probable.

Irradiation Effects

In-reactor rupture experience has indicated that neutron irradiation of a fuel element has important effects on its rupture behavior. Investigation of these effects under controlled conditions is difficult, and, at this time, only a little information is available. Two experimental approaches are currently underway; in-reactor ruptures of intentionally defected elements,[21] and out-of-reactor loop ruptures of previously irradiated fuel elements.[22] The first approach has not produced sufficient information as yet to permit conclusions in this report on the effects of irradiation.

In the second approach, irradiated fuel elements are defected with a 25 mil pinhole and are then ruptured in an out-of-reactor loop. The corrosion product oxide is caught on a filter in the loop. The activity increase of this filter is continuously recorded. These tests are being conducted by G. E. Neibaur, Coolant Systems Development Operation, who supplied activity buildup data for the following comparison with unirradiated rupture data.

Assuming the activity buildup on the loop filter is roughly proportional to the amount of uranium corroded, an activity based rupture curve is obtained in a manner similar to the hydrogen-based autoclave rupture curves. In

Figure 59 the rupture curve thus obtained of an irradiated rod element is compared to an unirradiated rupture. Both rods were beta-heat treated and water-quenched prior to exposure. One rod was irradiated in water at 270 C to an exposure of 1200 MWD/T. It was then ruptured (out-of-reactor) in water at 300 C, 1500 psig. For comparison, the rupture curve of an unirradiated, isothermal quenched* rod is also shown.

The irradiated rod ruptured at a rate less than the unirradiated water-quenched rod. The isothermal-quenched unirradiated rod ruptured at an even lower rate. The irradiated rod was autoclave proof tested at 400 C prior to exposure in the reactor. As mentioned in the discussion of heat treatment effects, the annealing which a water quenched element receives during the autoclave cycle slows its rupture rate to about the same as for an isothermally quenched element. The irradiated element should therefore be compared with the unirradiated isothermally quenched sample. The effect of irradiation is thus seen to increase the rupture rate. The increase in rupture rate due to irradiation appears to be associated with more rapid attack down the bond region, causing separation of the cladding or blistering. This would indicate that irradiation weakens the bond or makes it more susceptable to rapid hydrogen penetration. Notch-fracture tests performed by Goffard[18] indicate that irradiation does not weaken the bond, but in this author's opinion, it is not clear that the notch tests are truly indicative of the irradiated bond strength, or the porosity or chemical behavior of the bond layer.

Neibaur has found that fuel elements irradiated in cold water rupture two to six times faster than those irradiated in hot water.[22] This appears to be associated with more extensive cracking of the uranium core during cold water irradiation.

Comparison of In-Reactor and Autoclave Ruptures

Occasionaly an accidental rupture of a fuel element during irradiation in an in-reactor test loop provides an opportunity to compare "real" ruptures with "similated" ruptures produced in an autoclave. Agreement in visual appearance of these ruptures is good, indicating that autoclave-produced rupture data are valuable in predicting in-reactor behavior.

---

* Beta treated at 720 C for 10 minutes, held at 600 C for 10 minutes, then air-cooled.

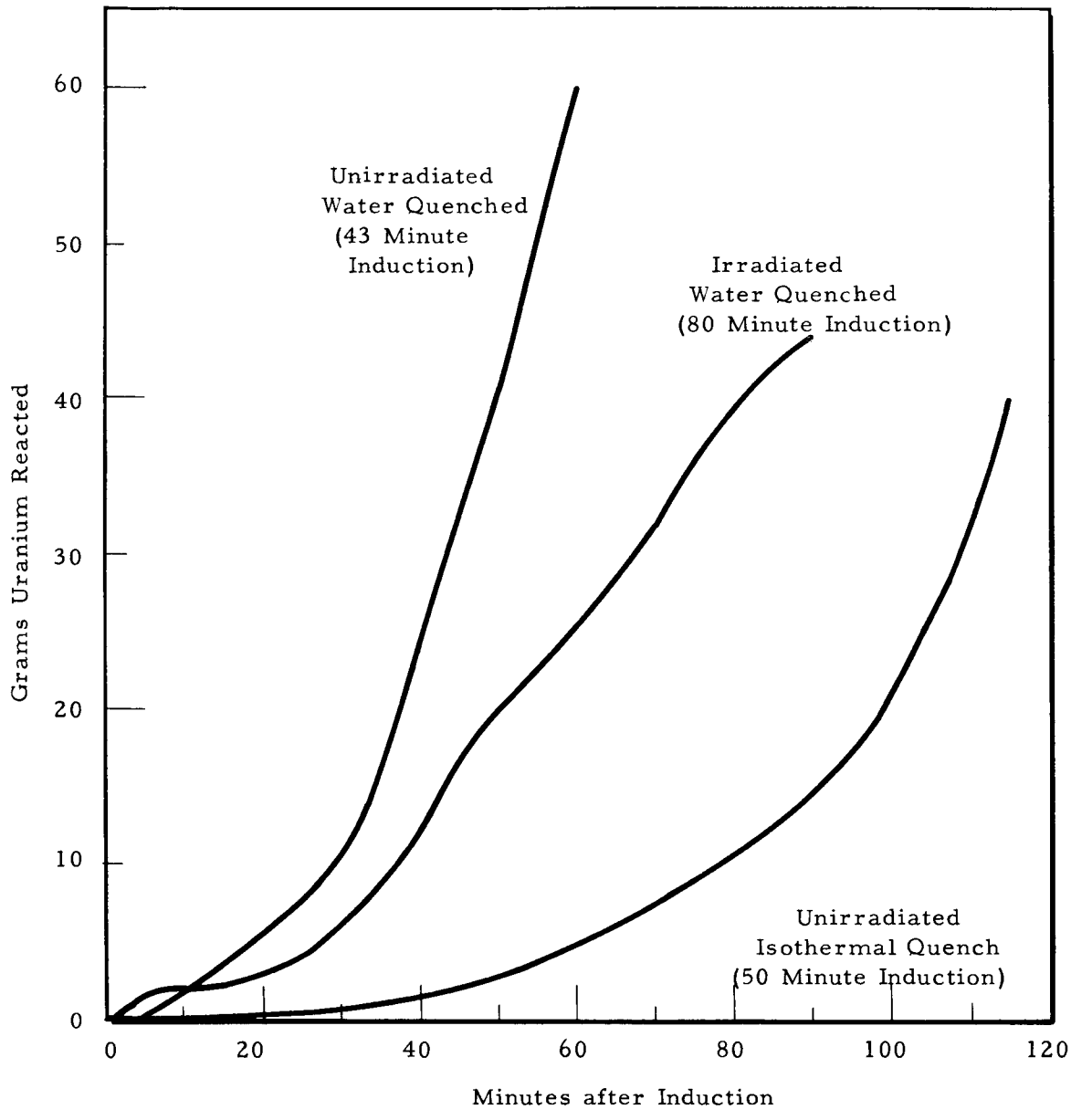

FIGURE 59

Irradiation Effect on 300 C Rupture

AEC-GE RICHLAND, WASH.

A small tubular element which failed after low exposure in-reactor is shown in Figure 60. The failure was apparently caused by corrosion pit penetration of the inner cladding in 300 C water. This failure is described in detail by G. A. Last and G. T. Geering.[23] This failure was simulated "in-autoclave" using a three-inch length of the same size element, with a 25-mil pinhole drilled through the inner cladding. The defected sample was autoclaved at 300 C, 1500 psig. After a 63-minute induction period, the cladding failed and the element ruptured at a rate of about 2.7 grams of uranium per minute. The rupture was stopped six minutes after induction. It is shown in Figure 61. The blister was larger than the one formed in-reactor because the autoclave failure was allowed to run until more of the uranium core had reacted. In all other respects, the autoclave rupture appeared the same as the in-reactor rupture.

A rod element which failed in-reactor at high exposure in about 300 C water is shown in Figure 62. At the site of the failure there were two bumps or blisters along the length of the split in the cladding. Swelling of the cladding extended from the blisters to halfway around the rod. An attempt to simulate this type of failure "in-autoclave" was made with a slot-defected rod sample. The results described in a previous section and shown in Figure 36 were not very similar to the in-reactor failure. While blisters formed at the slot, they did not extend around the fuel element. Another attempt to simulate this failure was made in which a sample element was heat-treated at 800 C for 16 hours to produce a thick weakened bond layer. The sample was pinhole-defected and ruptured in 300 C water. The result, shown in Figure 63, was quite similar to the in-reactor rupture. The cladding split lengthwise and the blisters extended partially around the rod. It appears that the in-reactor, high exposure, rupture characteristics are those of a weakened bond layer.

ACKNOWLEDGMENTS

Sincere appreciation is extended to J. W. Goffard of Fuel Element Design Operation for supplying the samples used in the study, and for valued discussions; to G. E. Neibaur of Coolant Systems Development Operation for supplying data on irradiated ruptures; and to O. L. Darling, Corrosion and Coatings Operation, for his assistance in performing the tests.

A Top View Section B Cross-Section

FIGURE 60

In-Reactor Tube Rupture

FIGURE 61

Autoclave "Simulated" Tube Rupture

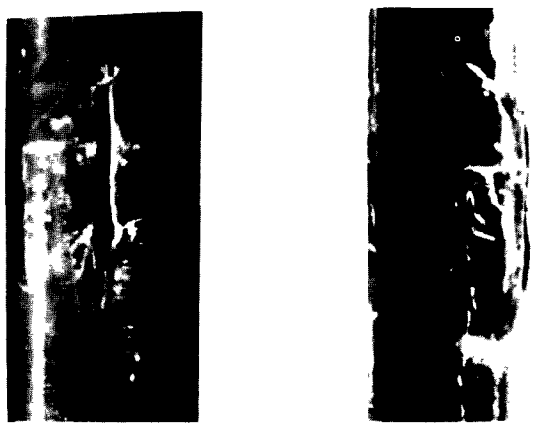

A Front B Profile

FIGURE 62

In-Reactor Rod Rupture

FIGURE 63

Autoclave "Simulated" Rod Rupture

REFERENCES

1. Draley, J. E. and J W. McWhirter. Aqueous Corrosion of Uranium and Its Alloys, ANL-4862. May, 1952.
2. Draley, J. E. and J. W. McWhirter. Effects of Metal Purity and Heat Treatment on the Corrosion of Uranium in Boiling Water, ANL-5029. April, 1953.
3. Schroeder, J. B., D. A. Vaughan and C. M. Schwartz. J. Electrochemical Soc., 106: 486. June, 1959.
4. Dillon, R. L. Unpublished Data.
5. Bowen, H. C., J. E. Minor and R. G. Post. Unpublished Data.
6. Johnson, O. and A. S. Newton. Chemical Research - Radiochemistry Report for Month Ending 11-6-43, CC-1063. 1943.
7. Burke, J. E. The Formation of Uranium Hydride, MCCD-280. 1946.
8. Troutner, V. H. Rupture Kinetics of Zircaloy Clad Fuel Elements in High Temperature Water and Steam - Interim Report No. 1, Experimental Methods and Procedures, HW-61378. August, 1959.
9. Troutner, V. H. Interim Report No. 2, Coextruded Rod Elements with Pinhole Defects, HW-61379. August, 1959.
10. Troutner, V. H. Interim Report No. 3, Mechanism of the Uranium-Water Reaction, HW-61799. September, 1959.
11. Troutner, V. H. Interim Report No. 4, Coextruded Tube Elements with Pinhole Defects and Various Annular Spacings, HW-62348. October, 1959.
12. Troutner, V. H. Interim Report No. 5, Comparison of In-Reactor and Ex-Reactor Ruptures, HW-62766. November, 1959.
13. Troutner, V. H. Interim Report No. 6, Effects of Carbon and Zirconium Content on Uranium Corrosion and Rupture Mechanisms, HW-63137. December, 1959.
14. Troutner, V. H. Interim Report No. 7, Reaction and Rupture Kinetics in Steam, HW-65493. September, 1960.
15. Troutner, V. H. Interim Report No. 8, Hydriding of Zircaloy Components and Comparison of Autoclave and Loop Experiments, HW-66926. September, 1960.
16. Troutner, V. H. A Versatile Autoclave Facility for Aqueous Corrosion Research, HW-64111. July, 1960.
17. Kittel, J. H., S. Greenberg, S. H. Paine and J. E. Draley. Nuclear Sci. and Eng., 2: 431-49. 1957.

18. Goffard, J. W. The Influence of the Bond on the Defect Test Behavior of Coextruded Zircaloy-2 Clad Uranium, HW-64194. July, 1960. CONFIDENTIAL.

19. Hayden, K. D. and J. W. Goffard. Defect Testing of Coextruded Uranium-Zircaloy-2 Clad Fuel Material in a 300 C Out-of-Reactor Recirculating Water Loop, HW-60039. September, 1959. CONFIDENTIAL.

20. Hayden, K. D. Coextruded Uranium and Zircaloy-2 Rupture Test with Internal Heat Generation, HW-60775. June, 1959. SECRET.

21. Call, R. L., et al. Interim Report: In-Reactor Rupture Testing of Zircaloy-2 Clad Seven-Rod Cluster Fuel Elements, HW-65009. May, 1960. CONFIDENTIAL.

22. Neibaur, G. E. Personal Communication.

23. Last, G. A. and G. T. Geering. Examination of Ruptured KER Tube-In-Tube Fuel Element from IP-250-A, HW-62428. October, 1959. SECRET.

24. Theide, R. A. Autoclave Testing of Zircaloy-2, HW-65350. June, 1960.

INTERNAL DISTRIBUTION

Copy Number

1	F. W. Albaugh - H. J. Pessl
2	W. K. Alexander
3	G. S. Allison
4	T. W. Ambrose
5	E. R. Astley
6	J. A. Ayres - K. D. Hayden - R. J. Lobsinger
7	J. M. Batch
8	J. L. Bates
9	J. H. Brown
10	S. H. Bush
11	J. J. Cadwell - E. A. Evans - J. C. Tobin
12	A. C. Callen
13	W. R. Conley - G. L. Rogers
14	R. L. Dickeman
15	D. R. Dickinson
16	R. L. Dillon
17	T. W. Evans
18	M. C. Fraser
19	R. M. Fryar - N. G. Wittenbrock
20	G. T. Geering - J. W. Weber
21	S. M. Gill - A. E. Guay
22	J. W. Goffard
23	O. H. Greager
24	J. W. Green
25	B. Griggs
26	W. Hamilton
27	H. Harty
28	W. H. Hodgson - W. A. Blanton
29	W. G. Hudson
30	M. E. Jackson
31	S. S. Jones
32	R. S. Kemper - E. A. Smith
33	W. K. Dratzer
34	G. A. Last
35	L. H. McEwen
36	N. R. Miller
37	J. E. Minor
38	G. E. Neibaur
39	R. Nilson
40	R. S. Paul
41	G. W. Riedeman
42	J. W. Riches
43	A. L. Ruis
44	A. Scott

INTERNAL DISTRIBUTION (contd.)

Copy Number	
45	D. E. Sebade - F. H. Sherwood
46	D. W. Shannon
47	R. A. Thiede
48	V. H. Troutner
49	R. E. Trumble
50	L. D. Turner
51	F. W. Van Wormer
52	P. C. Walkup
53	O. J. Wick
54	F. W. Woodfield
55	G. E. Zima
56	300 Files
57	Record Center
58 - 78	Extra
79 - 82	G. E. Technical Data Center, Schenectady

EXTERNAL DISTRIBUTION

Number of Copies	
2	Aberdeen Proving Ground
1	Aerojet-General Corporation
1	Aerojet-General Nucleonics
1	AFPR, Boeing, Seattle
2	AFPR, Lockheed, Marietta
2	ANP Project Office, Convair, Fort Worth
1	Alco Products, Inc.
1	Allis-Chalmers Manufacturing Company
1	Allis-Chalmers Manufacturing Company, Washington
1	Allison Division - GMC
10	Argonne National Laboratory
1	Armour Research Foundation
1	Army Ballistic Missile Agency
1	AEC Scientific Representative, Belgium
1	AEC Scientific Representative, France
1	AEC Scientific Representative, Japan
3	Atomic Energy Commission, Washington
4	Atomic Energy of Canada Limited
4	Atomics International
4	Babcock and Wilcox Company
2	Battelle Memorial Institute
1	Beryllium Corporation
1	Bridgeport Brass Company
1	Bridgeport Brass Company, Adrian

EXTERNAL DISTRIBUTION (contd.)

Number of Copies	
2	Brookhaven National Laboratory
1	Brush Beryllium Company
1	Bureau of Mines, Albany
1	Bureau of Ships (Code 1500)
1	Carborundum Company
3	Chicago Operations Office
1	Chicago Patent Group
1	Clevite Corporation
1	Combustion Engineering, Inc.
1	Combustion Engineering, Inc. (NRD)
1	Convair-General Dynamics Corporation, San Diego
1	Defence Research Member
1	Denver Research Institute
2	Department of the Army, G-2
1	Dow Chemical Company (Rocky Flats)
4	duPont Company, Aiken
1	duPont Company, Wilmington
1	Frankford Arsenal
1	Franklin Institute of Pennsylvania
2	General Atomic Division
2	General Electric Company (ANPD)
2	General Electric Company, St. Petersburg
1	General Nuclear Engineering Corporation
1	Glasstone, Samuel
1	Goodyear Atomic Corporation
1	Grand Junction Operations Office
2	Iowa State University
2	Jet Propulsion Laboratory
1	Johns Hopkins University (ORO)
3	Knolls Atomic Power Laboratory
3	Los Alamos Scientific Laboratory
1	Los Alamos Scientific Laboratory (Sesonske)
1	M & C Nuclear, Inc.
2	Mallinckrodt Chemical Works
1	Maritime Administration
1	Martin Company
1	Mound Laboratory
1	NASA Lewis Research Center
2	National Bureau of Standards
1	National Bureau of Standards (Library)
1	National Carbon Company
2	National Lead Company of Ohio
3	Naval Research Laboratory
1	New Brunswick Area Office
1	New York Operations Office

EXTERNAL DISTRIBUTION (contd.)

Number of Copies	
1	Northern Research and Engineering Corporation
1	Nuclear Development Corporation of America
1	Nuclear Materials and Equipment Corporation
1	Nuclear Metals, Inc.
1	Oak Ridge Institute of Nuclear Studies
2	Office of Naval Research
1	Office of Naval Research (Code 422)
1	Olin Mathieson Chemical Corporation
1	Ordnance Materials Research Office
1	Ordnance Tank-Automotive Command
1	Patent Branch, Washington
4	Phillips Petroleum Company (NRTS)
1	Picatinny Arsenal
1	Power Reactor Development Company
3	Pratt and Whitney Aircraft Division
1	Rensselaer Polytechnic Institute
2	Sandia Corporation, Albuquerque
1	Stevens Institute of Technology (Comstock)
1	Sylvania Electric Products, Inc.
1	Technical Research Group
1	Tennessee Valley Authority
1	Union Carbide Metals Company
2	Union Carbide Nuclear Company (ORGDP)
5	Union Carbide Nuclear Company (ORNL)
1	Union Carbide Nuclear Company (Paducah Plant)
1	USAF Project RAND
1	U. S. Geological Survey, Denver
1	U. S. Geological Survey, Menlo Park
1	U. S. Geological Survey, Washington
1	U. S. Naval Postgraduate School
1	U. S. Patent Office
2	University of California, Berkeley
2	University of California, Livermore
1	University of Puerto Rico
1	Watertown Arsenal
4	Westinghouse Bettis Atomic Power Laboratory
1	Westinghouse Electric Corporation
8	Wright Air Development Division
1	Yankee Atomic Electric Company
325	Office of Technical Information Extension
75	Office of Technical Services, Washington

EXTERNAL DISTRIBUTION (Special)

2	HOO Technical Information Library